การหาความเสถียรทางความร้อนของผลึกเดี่ยวระดับนาโนเมตร

โคบอลต์อะลูมิเนต ซิงก์อะลูมิเนต และนิเกิลอะลูมิเนต

นางสาว อังคณา กันยานุชรัตน์

วิทยานิพนธ์นี้เป็นส่วนหนึ่งของการศึกษาตามหลักสูตรปริญญาวิศวกรรมศาสตรมหาบัณฑิต

สาขาวิชาวิศวกรรมเคมี ภาควิชาวิศวกรรมเคมี

คณะวิศวกรรมศาสตร์ จุฬาลงกรณ์มหาวิทยาลัย

ปีการศึกษา 2544

ISBN 974-03-1344-2

DETERMINATION OF THE THERMAL STABILITY OF $CoAl_2O_4$, $ZnAl_2O_4$ AND $NiAl_2O_4$ SINGLE NANOCRYSTALS

Miss Angkana Kanyanucharat

A Thesis Submitted in Partial Fulfillment of the Requirements
For the Degree of Master of Engineering in Chemical Engineering
Department of Chemical Engineering
Faculty of Engineering
Chulalongkorn University
Academic Year 2001

ISBN 974-03-1344-2

Thesis Title

Thesis Title	Determination of the thermal stability of $CoAl_2O_4$, $ZnAl_2O_4$ and $NiAl_2O_4$ single nanocrystals
By	Miss Angkana Kanyanucharat
Field of study	Chemical Engineering
Thesis Advisor	Professor Piyasan Praserthdam, Dr.Ing.
Thesis Co-advisor	Miss Waraporn Tanakulrungsank, D.Eng.

Accept by the Faculty of Engineering, Chulalongkorn University in Partial Fulfillment of the Requirements for the Master's Degree

..... Dean of Faculty of Engineering
(Professor Somsak Panyakeow, D.Eng.)

Thesis Committee

..... Chairman
(Associate Professor Ura Pancharoen, D.Eng.Sc.)
..... Thesis Advisor
(Professor Piyasan Praserthdam, Dr.Ing.)
..... Thesis Co-advisor
(Waraporn Tanakulrungsank, D.Eng.)
.....
(Suphot Phatanasri, D.Eng.)
.....
(Assistant Professor M.L. Supakanok Thongyai, Ph.D.)

อังคณา กันยานุชรัตน์: การหาความเสถียรทางความร้อนของผลึกเดี่ยวระดับนาโนเมตรโคบอลต์อะลูมิเนต ซิงก์อะลูมิเนต และนิเกิลอะลูมิเนต (DETERMINATION OF THE THERMAL STABILITY OF $CoAl_2O_4$, $ZnAl_2O_4$ AND $NiAl_2O_4$ SINGLE NANOCRYSTALS) อ. ที่ปรึกษา: ศ.ดร.ปิยะสาร ประเสริฐธรรม, อ.ที่ปรึกษาร่วม: อ.ดร.วราภรณ์ ธนะกุลรังสรรค์, 93 หน้า. ISBN 974-03-1344-2

การศึกษานี้เป็นการสังเคราะห์ผลึกสไปเนล (โคบอลต์อะลูมิเนต ซิงก์อะลูมิเนต และนิเกิลอะลูมิเนต) ด้วยวิธีโซลโวเทอร์มอลในสารละลายโทลูอีนโดยทำการสังเคราะห์ที่อุณหภูมิแตกต่างกัน อัตราส่วนของโคบอลต์ ซิงก์และนิเกิลต่ออะลูมินัมเท่ากับ 0.5 ทำการวิเคราะห์ผลึกที่ได้จากการสังเคราะห์โดยวิธีการกระเจิงรังสีเอ็กซ์ (X-ray diffraction) กล้องจุลทรรศน์อิเล็กตรอนแบบส่องผ่าน (Transmission Electron Microscopy) และการวัดพื้นที่ผิว (BET surface area) ความเสถียรทางความร้อนนิยามว่าคืออัตราส่วนของพื้นที่ผิวของผลึกหลังการเผาต่อพื้นที่ผิวของผลึกที่ได้จากการสังเคราะห์ หรือ อัตราส่วนของขนาดผลึกหลังการเผาต่อขนาดผลึกก่อนการเผา จากการศึกษาพบว่าผลึกแต่ละชนิดที่ได้จากการสังเคราะห์และการเผาเป็นผลึกเดี่ยวระดับนาโนเมตรและมีโครงสร้างเป็นสไปเนลโดยไม่มีเฟสอื่นเจือปน ขนาดผลึกและพื้นที่ผิวขึ้นอยู่กับอุณหภูมิในการเผาและอุณหภูมิในการสังเคราะห์ จากผลสรุปที่ได้พบว่า อุณหภูมิในการสังเคราะห์และอุณหภูมิในการเผามีผลต่อความเสถียรทางความร้อนของโลหะอะลูมิเนตสปเนลแต่ละชนิด แสดงได้จากการเปลี่ยนแปลงของขนาดผลึกและพื้นที่ผิว การเปลี่ยนไอออนที่มีประจุ 2+ (โคบอลต์ 2+ ซิงก์ 2+ และนิเกิล 2+) ในตำแหน่งเตตระฮีดรอลของโลหะ อะลูมิเนตสไปเนลส่งผลต่อความเสถียรทางความร้อนของผลึกโดยเรียงลำดับความเสถียรทางความร้อนได้ดังนี้ นิเกิลอะลูมิเนต > โคบอลต์อะลูมิเนต > ซิงก์อะลูมิเนต ซึ่งเป็นผลเนื่องมาจากพลังงานพันธะโลหะกับออกไซด์และการกระจายตัวของประจุบวกบนตำแหน่งเตตระฮีดรอลในโครงสร้างสไปเนล

ภาควิชา...วิศวกรรมเคมี..... ลายมือชื่อนิสิต.....

สาขาวิชา...วิศวกรรมเคมี..... ลายมือชื่ออาจารย์ที่ปรึกษา.....

ปีการศึกษา...2544..... ลายมือชื่ออาจารย์ที่ปรึกษาร่วม.....

#4370382621: MAJOR CHEMICAL ENGINEERING
KEYWORD: SOLVOTHERMAL / SPINEL / THERMAL STABILITY
ANGKNA KANYANUCHARAT: DETERMINATION OF THE THERMAL STABILITY OF $CoAl_2O_4$, $ZnAl_2O_4$ AND $NiAl_2O_4$ SINGLE NANOCRYSTALS. THESIS ADVISOR: PIYASAN PRASERTHDAM, Dr.Ing. THESIS CO-ADVISOR: WARAPORN TANAKULRUNGSANK, D.Eng. 93 pp. ISBN 974-03-1344-2

The synthesis of spinel type mixed oxides ($CoAl_2O_4$, $ZnAl_2O_4$, and $NiAl_2O_4$) by solvothermal method was studied using toluene as a solvent at various reaction temperatures for 2h. The molar ratio of Co/Al, Zn/Al, and Ni/Al was 0.5. The powder obtained from air dried was characterized by X-ray diffraction (XRD), Transmission Electron Microscopy (TEM) and BET surface area measurement. The thermal stability was defined by the ratio of BET surface area of product after calcined (m^2/g) to BET surface area of as-synthesized product (m^2/g), and the ratio of the crystallite size of calcined product (nm) to the crystallite size of as-synthesized product (nm). Each particle of spinel products was single crystal and was formed without any contaminated phase. The crystallite size and surface area properties depended on the calcination temperature and the reaction temperature in the synthesis. It was found that the reaction temperature in the synthesis and the calcination temperature affected the thermal stability of each metal aluminate spinels that result in the change of crystallite size and BET surface area. The varying of divalent ions (Co^{2+}, Zn^{2+} and Ni^{2+}) in tetrahedral sites of metal aluminate spinels affected the thermal stability. The thermal stability of the metal aluminate spinel revealed in the order of, $NiAl_2O_4 > CoAl_2O_4 > ZnAl_2O_4$. That is the result of the difference in bond dissociation energy of metal oxides and cation distribution over sites with tetrahedral coordination in the spinel-type structure.

Department...Chemical Engineering.....
Field of study...Chemical Engineering.....
Academic year...2001.....

Student's signature.....
Advisor's signature.....
Co-advisor's signature.....

ACKNOWLEDGEMENT

The author would like to express her greatest gratitude to her advisor, Professor Dr. Piyasan Praserthdam, for their invaluable guidance throughout this study. Special thanks for Dr. Waraporn Tanakulrungsank, her co-advisor, for her kind supervision in this thesis. She would also gratefully thank to Associate Professor Dr. Ura Panchareon, as the chairman, and Assistant Professor Dr. Supakanok Thongyai, and Dr. Suphot Phatanasri, members of the thesis committee.

Many thanks for kind suggestion and useful help to Mr. Orkorn Mekasuvandamrong, Mr. Choowong Chaisuk, Miss Bongkot Ngamsom, Miss Sirarat Kongwudthiti, Miss Paveena Sangthonganothai, Mr. Mongkolchanok Pramottana and many friends in the Petrochemical Laboratory who always provide the encouragement and co-operate along the thesis study.

Finally, she also would like to dedicate this thesis to her parents who have always been the source of her support and encouragement.

CONTENTS

Page

CONTENTS (CONT.)

Page

LIST OF TABLES

Table **Page**

LIST OF FIGURES

Figure **Page**

LIST OF FIGURES (CONT.)

Figure **Page**

LIST OF FIGURES (CONT.)

Figure **Page**

LIST OF FIGURES (CONT.)

Figure **Page**

INTRODUCTION

In this research study, the focus is spinel-type structure, which is a structure of catalyst. These spinel-type structures have a generation formula AB_2O_4, in which A is a divalent metal and B is a trivalent one. Spinels are usually synthesized at high temperature from a mixture at solid state of the two oxide components. In these spinel-type structures, the metal aluminates seem to be a good option because of their properties such as greater thermal stability, high resistance to acids and alkalis, hydrophobicity, low surface acidity, high melting points and surface area, lower temperature sinterability, increase hardness, ductility, better diffusion, etc. [1]. These properties make them interesting materials as catalysts and carriers for active metals to substitute the more traditional systems.

In this study, the transition metals of the first series in Periodic Table, which are Scandium (Sc), Titanium (Ti), Vanadium (V), Chromium (Cr), Manganese (Mn), Iron (Fe), Cobalt (Co), Nickel (Ni), Copper (Cu) and Zinc (Zn), are varied in tetrahedral sites of the spinel-type structure of metal aluminate spinels. Cobalt aluminate, zinc aluminate and nickel aluminate spinels could be formed by the solvothermal method.

Furthermore, cobalt aluminate ($CoAl_2O_4$) has a normal spinel structure in which Co^{2+} are accommodated in tetrahedral positions while Al^{3+} ions are in octahedral positions. $CoAl_2O_4$ has received special interest due to their technological applications as inorganic ceramic blue pigment [2-5]. $CoAl_2O_4$ is also of great interest in the field of heterogeneous catalysis while it has been used for catalytic application [6,7]. Recently, $CoAl_2O_4$ has been prepared by several methods, such as co-precipitated method [8,9], sol-gel method [4,7,10], hydrothermal method [2] and polymerized complex methods [2].

Zinc aluminate ($ZnAl_2O_4$) has a normal spinel structure in which Zn^{2+} are accommodated in tetrahedral positions, while Al^{3+} are in octahedral positions. $ZnAl_2O_4$ tend to prevent sintering of noble metals due to a strong metal-support interaction [8,11-13]. The sintering resistance and chemical stability of catalytically phases are the very important problems for high-temperature processes. $ZnAl_2O_4$ has received attention as a ceramic material. Moreover, it has been used as a catalyst for double bond isomerization process of alkenes [8,12], for the dehydrogenation of saturated alcohols to olefins [8], preparation of polymethylbenzenes [8], methanol and

higher alcohols synthesis [8], or the synthesis of styrenes from acetophenones [12] and foremost as a support for alkane dehydrogenation catalyst [12]. Presently, $ZnAl_2O_4$ has been prepared by several methods, such as high temperature calcination of mixed aluminium and zinc oxides [12], co-precipitated method [12,14], sol-gel method [11,14,15], hydrothermal method [12,16] and the solution combustion method [3].

In addition, Nickel aluminate ($NiAl_2O_4$) has a normal spinel structure in which Ni^{2+} are accommodated in tetrahedral positions, while Al^{3+} are in octahedral positions. Several studies on alumina-supported nickel catalysts [17] have shown the formation of nickel aluminate spinel, $NiAl_2O_4$, which has an important effect on final catalyst. It seems that these systems have well-dispersed nickel species on their surface [17]. The $NiAl_2O_4$ spinels were synthesized at low temperatures in order to be used as supports of nickel catalysts for the hydrodechlorination of 1,2,4-trichlorobenzene in gas phase [17]. $NiAl_2O_4$ supports, on which could form a stable nickel supported were more resistant to deactivation by coke formation during the reforming of methane and acetylene hydrogenation processes than other supports [18]. The preparation of $NiAl_2O_4$ has various methods such as co-precipitated method [17], sol-gel method [19,20] and the solution combustion method [3].

As mentioned above, the advantage for $CoAl_2O_4$, $ZnAl_2O_4$ and $NiAl_2O_4$ of preparation methods is quasi-atomic dispersion of component cations in liquid precursors, which facilitate synthesis of the crystallized powder with nanosize and high purity at low temperature [2].

The properties of powder may vary as different preparation methods are used [2]. So, the desired properties of final material are been used as principle in the selection of preparation methods. The solvothermal method was applied from hydrothermal method using the solvent instead of water in the synthetic process. This preparation method had been developed the novel method by Inoue et al. [21-24]. In this study, the novel method has been used in the synthesis of cobalt aluminates and zinc aluminates. In this research, great interest has focused the comparison thermal stability and nanocrystallite sizes of spinel-type structure between group VIIIB and group IIB, which were varied the elements in the form of some aluminate spinels in the same row (i.e., Co, Ni and Zn metals). However, there is comparison between metal oxides as well**.**

The present study is arranged as follow:

Chapter II presented literature reviews of novel synthesis of metal oxides in several solvents

Chapter III explained the relatively theory about this research. The properties of spinels and metal oxides were included in this chapter.

Chapter IV shows the experimental equipment, system and catalyst preparation.

Chapter V exhibits the experimental results of characterized catalysts. The X-Ray Diffraction (XRD) patterns, BET surface area, crystallite sizes and morphology are shown.

In the last chapter, the overall conclusions were developed from this research is given.

Finally, The samples of calculation for the catalyst preparation and crystallite size are included in appendices at the end of this thesis.

LITERATURE REVIEWS

For this work, the materials are studied as spinels ($CoAl_2O_4$, $ZnAl_2O_4$ and $NiAl_2O_4$) and metal oxides (CoO, ZnO and NiO). These materials are synthesized several methods as followed

Normally soft chemical routes like sol-gel [4,14,19], microemulsion [20] and templating techniques [3] are used to prepared porous nanocrystalline materials. However, these methods are involved and require expensive metal alkoxide precursors and efficient templating agents. However, There are many synthesized methods of metal oxides and binary oxides.

T. Ohgushi and S. Umeno studied low temperature synthesis of dispersed fine particle of cobalt aluminate that is a new application of zeolite. They found $CoAl_2O_4$, with the spinel structure in a dispersed form, was synthesized at 400°C by using zeolite A as a staring material. A specific surface area of products was measured by adsorption of $(CH_3)_2CHCH_3$ gas at -110°C and the mean size of the product particles was estimated to be about 14 nm. Zeolites have been used as catalyst, adsorbent or ion exchangers owing to their porous structure. In the applications, the zeolite structure is, of course, preserved. In the present work, zeolite A was used as a source of aluminium for the synthesis of cobalt aluminate [25].

F. Mayer et al. searched size-controlled synthesis of nanoscaled aluminium spinels using heterobimetallic alkoxide precursors via water/oil microemulsions. They prepared nanosized spinels of type MAl_2O_4 (M = Mg, Co, Ni, Cu) by a sol-gel type hydrolysis of alkoxides in the inverse micelles of w/o microemulsions. Heterobimetallic alkoxides $M[Al(OPr^i)_4]_2$ containing both metallic elements in the desired stoichiometric in the molecules was established by single crystal X-ray diffraction analysis. By varying the hydrophilic chain length of detergent, the diameter of the water droplets can be tuned in the nanometer range, as determined by dynamic light scattering. The size of the resulting spinel nano-particles as evaluated from XRD peak profile analysis, correlates to the droplet

size. The results of ceramic syntheses using the different types of alkoxide precursors were compared which reveal the advantage of a single source approach [20].

W. S. Cho and M. Kakihana synthesized ceramic pigment $CoAl_2O_4$ nanocrystals by a polymerized complex technique. Cobalt nitrate, aluminum nitrate, citric acid and ethylene glycol were used as precursor materials. The formation of pure crystallized $CoAl_2O_4$ nanocrystals occurred when the precursor was heat-treated at 350°C in air for 2 h. They propose a model for $CoAl_2O_4$ formation from the polymeric precursor. The model contains a series of steps such as the transformation of the precursor to amorphous cobalt aluminate, three-dimensional nucleation and growth, and solid-state reaction [2].

S. Chamlal et al. prepared cobalt spinel $CoAl_2O_4$ by the technique of colloidal solution destabilization using as the sol-gel process. The powder obtained from the dried gel was characterized by thermal analysis (Thermogravimetric and differential), X-ray diffraction, infrared spectroscopy, and specific surface properties (surface charge and electrophoretic mobility) of the spinel powder fired at 600°C, in suspension in different eletrolite solutions (10^{-3} molar ionic strengt), shows that the spinel material charge depends on the pH of solution. The spinel sol was used for the preparation of membrane by the slip-casting method [10].

M. Zayat and D. Lavy prepared bright blue $CoAl_2O_4$ particles by the sol-gel and citrate –gel methods using aluminum *sec*-butoxide, cobalt salts and citric acid as oxides precursors. Both methods start from sols of the precursor alkoxides and salts, and involve formation of heterogeneous solid intermediates, reducing atomic diffusion processes during thermal treatment. This important feature results in a substantial lowering of the time and temperature needed for the formation of the desired compounds. The stages of the formation of $CoAl_2O_4$, as well as the characterization of the resulting compounds were done using XRD, FTIR, UV-VIS, SEM, and TGA/DTA techniques. The structure, coloration, particle size, and temperature of formation of the resulting $CoAl_2O_4$ phases were

found to depend on the precursors and methods used for preparation and the calcination temperature. The lowest temperature for preparation of the blue cobalt aluminate of about 700°C was obtained using the citrate-gel method. This temperature is much lower than that needed for preparation of the compound through traditional solid-state reactions (above 100°C) [12].

T. Mimani prepared nanocrystalline metal aluminates MAl_2O_4, M = Mn, Cu and Zn by combustion of aqueous solutions containing corresponding metal acetate, aluminium nitrate, ammonium nitrate and different fuels, e.g. urea / carbohydrazide / oxalyldihydrazide / hexamethylenetetramine / glycine. The spinels obtained are nanosize (10-80 nm) oxides with surface area varying from 40 to 180 m^2/g depending upon the fuel used. The products have been characterized by powder XRD and Al MAS NMR spectroscopy. The particulate and morphological properties have been investigated using TEM and SEM techniques. Both $ZnAl_2O_4$ and $CuAl_2O_4$, prepared with carbohydrazide and glycine fuels are porous [3].

Y. Cesteros et al. synthesized nickel spinels at low temperature to be use as nickel catalyst supports for hydrodechlorination of 1,2,4-trichlorobenzene in the gas phase. All the samples were structurally characterized using X-ray diffraction (XRD), BET, temperature-programmed reduction (TPR), scanning electron microscopy (SEM) and temperature-programmed desorption (TPD) techniques. The $Ni/NiAl_2O_4$ catalysts test had high conversions and selectivities towards benzene. This is due to their reduction degree (XRD) and structural surface properties (BET area, SEM, TPD). The most active and selective catalyst yields 87% benzene at 523 K for a conversion of 82%. These Ni/spinel cayalysts desorb large amounts of hydrogen at lower temperatures (<625 K), which can complete with the aromatic compounds to be adsorbed on the surface of the catalyst. The amount of low-temperature hydrogen and the fact that it completes with the aromatic molecules favour a more exhaustive hydrodechlorination [17].

C. Otero Areán et al. prepared high surface area nickel aluminate spinels by a sol-gel method. The oxide spinel $NiAl_2O_4$ and spinel-type solid solutions Al_2O_3- $NiAl_2O_4$ (at Ni/Al = 1:4, and Ni/Al = 1:8) were prepared by controlled hydrolysis of mixed metal alkoxides, followed by calculation of the resulting gels. Powder X-ray diffraction showed that all samples prepared were single phase cubic materials having the spinel-type structure. The cubic lattice parameter, a_0, was found to decrease gradually with increasing aluminium content of the mixed metal oxides. The specific surface area (determined by nitrogen adsorption at 77 K) was found to be in range of 200-300 m^2g^{-2}. The materials were found to be basically mesoporous, the most frequent pore radius being in the range 3.2-6.4 nm. IR spectroscopy of CO adsorbed at liquid nitrogen temperature gave a main band at 2186-2195 cm^{-1}, which was assigned to the C-O stretching vibration of surface Al^{3+} …CO adducts where coordinatively unsaturated Al^{3+} ions act as Lewis acid centres [7].

M. A. Valenzuela et al. prepared zinc aluminate by the coprecipitation method from nitrate parent salts at 50°C and variable pH (from 2 to 7.5)[3,9]. Ammonium carbornate was used as precipitating agent. The synthesized zinc aluminate had a specific surface area of 20 m^2g^{-2} and pore volume of 0.15 ml g^{-1}. And then, $ZnAl_2O_4$ support was impregnated using aqueous solutions of H_2PtCl_2. It was tasted for isobutane dehydrogenation [11].

M. Zawadzki et al. prepared the zinc aluminate by hydrothermal method. The precursors for the hydrothermal synthesis were basic aluminium nitrate and hydrated zinc acetate [12].

However, Hydrothermal method is used for the synthesis of variety of ceramic materials [26-28]. Inoue et al. have developed novel method for the synthesis of several metal oxides inorganic media (non-aqueous solution). These methods have the advantage that the products consist of microcrystalline particles but are sufficiently high thermal stability; they still remain large surface areas after post-calcination at even higher temperature.

Inoue et al. [29] reported that the thermal reaction of gibbsite in ethylene glycol at 250°C yielded an ethylene glycol derivative of boehmite, in which organic moiety is incorporated covalently between the layer structures of boehmite. This reaction has been extended to the reaction of gibbsite in higher homologues of ethylene glycol, and they have found that microcrystalline alumina is formed under quite mild condition [22]. The synthetic process as mentioned above, the use of glycol (organic solvent) instead of water in the synthetic system is different method from the conventional methods. ***"Glycothermal method"*** was called for this synthesis method.

Inoue et al. [23] also that this reaction inert organic solvents such as toluene, benzene and/or others, thermal decomposition of aluminum alkoxide occurred and yielded a product compose of 4 to 20 nm particles having the alumina mixture. The alumina was stable and maintained a surface area above 100 m^2g^{-2} until its transformation at 1150°C to be α-alumina. With this result, they have applied this method for zirconia synthesis and reported that thermal decomposition of zirconium alkoxides in organic solvents yielded tetragonal zirconia, which had a large surface area and a fairly high thermal stability. However, zirconium n-alkoxide, which decomposed into glycols, did not decompose at 300°C in inert organic solvent [24]. Therefore they tried to hydrolyze the zirconium n-alkoxide in the inert organic solvent with a limited amount of water dissolved in the solvent from the gas phase and found that this method gave microcrystalline monoclinic zirconia having a much higher thermal stability [30].

Recently, Inoue et al. [21] reported that microcrystalline binary oxide were directly formed when a mixture of two alkoxides, acetylacetonate, and/or acetates was heated in 1,4-butandiol at elevated temperature under autogeneous pressure of the glycol (glycothermal reaction). An example was synthesis of gadolinium gallium garnets (GGG) by reaction of mixed gallium acetylacetonate with gadolinium acetate. This reaction has been extended to the reaction of a stoichiometric mixture of aluminium isopropoxide (AIP) and yttrium acetate, and found that crystalline

yittrium aluminium garnet (YAG) is formed under similar condition. No other phases were detected. The uncalcined YAG had a large surface area (107 m^2g^{-2}), which decreased to 44 m^2g^{-2} and 10 m^2g^{-2} after calcinations at 1000°C and 1300°C. YAG was composed of agglomerates of almost spherical particle size of approximately 30 nm. The use of ethylene glycol instead of 1,4-butanediol in the synthetic system afforded amorphous product [31].

Inoue et al. [32] have studied the reaction of aluminium isopropoxide (AIP) and other rare earth acetates. They reported that the reaction of AIP and acetates of the lanthanide elements from Gd to Lu in 1,4-butanediol at 300°C yielded the corresponding lanthanide aluminium garnets. The reaction of AIP with samarium or europium acetate gave a mixture of the corresponding garnets phase and lanthanide acetate oxide ($REOOCOCH_3$). However, the reaction of AIP with neodymium acetate gave only neodymium acetate oxide as the sole crystalline product.

As described above, samarium and europium garnets have never been reported except as solid solutions with YAG, and this paper is the first report of the synthesis of these garnets. Because of the metastability of these garnets, thermal methods such as ceramic processes of would not give these garnets. Ease in crystallization of the perovskite phase seems to be another reason for difficulty in the synthesis of these garnets by the thermal methods.

The stability of lanthanide hydroxide under the hydrothermal conditions increases in ionic size of the lanthanide element. This may be one reason for the increase in lower temperature limit for the hydrothermal synthesis of aluminium garnet with the increase in ionic size of the lanthanide element. The aluminium garnet with the large-size lanthanide ion hydrothermally prepared so far was $Tb_3Al_5O_{12}$ and $Gd_3Al_5O_{12}$ could not be prepared by the hydrothermal method. Since the ionic size of samarium and europium are still larger than gadolinium, there seems to be no possibility that samarium and europium garnets can be prepared by the hydrothermal method.

The previous paper as mentioned above, glycothermal treatment of microcrystalline gibbsite yield -alumina at 280°C, a much lower temperature than the alumina formation temperature by the hydrothermal method. The difference between glycothermal and hydrothermal reaction was attributed to the difference in stabilities of the intermediate phases, i.e. the glycol derivative of boehmite vs. well-crystallized boehmite. Similarly, the success if the synthesis of samarium and europium garnets by the glycothermal method may be attributed to the instability of intermediate species. Under glycothermal, aluminium alkoxide is easily converted to glycoxide. Thermal decomposition of the glycoxide molecule proceeds by intramolecular participation of the remaining hydroxyl group of glycol moiety, yielding an Al-O^- anion. In the absence of RE acetate, neucleophilic attack of this aluminate ion on another glycoxide molecule takes place, finally yielding the glycol derivative of boehmite. In the prescence of RE acetate, this aluminate anion attacks the RE ion forming the Al-O-RE bond, which finally yields the garnet crystals under the glycothermal conditions.

For the synthesis catalyst and catalyst supports, metal alkoxides are widely used as the starting material to avoid contamination of the inorganic counter anion from the corresponding metal salts, which affects the activity, and selectivity of the catalyst. In a series of Inoue's studies on the use of organic media in inorganic synthesis [16-20], metal alkoxides are used as the starting material and the effect of the structure of the alkyl group in the starting alkoxide was examined. They have found that the formation of the product required direct cleavage the C-O bonds in alkoxides, and therefore the thermal stability of C-O bonds may be a decisive factor for decomposition of metal alkoxide.

In the previous paper, Inoue et al. [21] found that thermal decomposition of titanium acetylacetonate in toluene at 250°C yielded nanocrystalline anatase titanium (IV) oxide (anatase titania) free from counter anion contamination, and that the sample calcine at 550°C had relatively high surface area (>50 m^2g^{-1}). Kominami et al. [33] reported that nanocrystalline anatase titanium (IV)

oxide prepared by the reaction of titanium (IV) tetra-tert butoxide using inert organic solvents at 300°C under autoclave condition. The yielded product was nanocrystalline anatase titanium (IV) oxide with a crystallite size of ca. 9 nm and a surface area of >100 m^2g^{-1}. The product was produced by this method was called as " TD-TiO_2 " (Thermal decomposition -Titania). The titanium (IV) oxide prepared from titanium (IV) tetra-tert butoxide by this manner was thermally stable upon calcination in air retained high surface area of ca. 100 m^2g^{-2} even after calcination at 550°C.

They also found that primary and secondary alkoxide of titanium (IV) were not decomposed under similar condition indicating that the thermal stability of C-O bonds in the alkoxides was a decisive factor for their decomposition. On the other hand, when water was fed in the autoclave separately from the organic solvent, the alkoxides was hydrolyzed at high temperature with water dissolved in the organic solvent from gas phase and thereby nanocrystalline titanium (IV) oxide was produced. The product prepared by this method was called as "HyCOM – TiO_2" (Hydrothermal Crystallization in Organic Media - Titania) [34,35]. In this HyCOM method, the structure of alkyl group was not a decisive factor for the TiO_2 formation. The resulting highly crystallized nanoparticles also exhibited highest, as far as they examined photocatalytic activity in several reaction systems [36-38].

Many papers as mentioned above, the synthesis of several metal oxides and binary metal oxides in organic solvents are explained. The product produced by this novel method has a large surface and high thermal stability. This novel method may be a new route to prepared micro- and nanocrystalline metal oxides [39,40]. The choice of the solvent, reaction conditions and structure of the alkyl group of the metal alkoxides can control physical properties of the product.

THEORY

This Chapter is explanation about the theory that mentioned physical and chemical properties of required studying the spinels and metal oxides, advantage and concerned knowledge with this work.

3.1 Aluminum [41]

Aluminum (Al) is a silver-white metallic element in group IIIA of Periodic Table having an electronic configuration of $1s^2 2s^2 2p^6 3s^2 3p^1$. Aluminum exhibits a valance of +3 in all compounds except high temperature gaseous species in which the aluminum may be monovalant or divalant. Nearly all rocks, particularly igneous rocks, contain aluminum as aluminosilicate minerals.

The properties of aluminum vary significantly to purity and alloying.

- Physical properties for aluminum of 99.99% purity

Physical properties for aluminum of 99.99% purity are summarized in Table 3.1. Although, a number of radioactive isotopes have been artificially produced, naturally occurring aluminum consists of a single stable isotope. Aluminum crystallizes in the face-centered cubic system having a unit cell of 0.40496 nm at 20°C. The unit cell contains four atoms and has coordination number of 12. The distance of closest approach of atoms is 0.2863 nm.

- Chemical properties

Aluminum reacts with oxygen, O_2 having a heat of reaction of –1675.7 kJ/mol (-400.5 kcal/mol), Al_2O_3 produced.

Table 3.1 Physical properties of aluminum

Property	Value
atomic number	13
atomic weight	26.9815
density at 25°C, kg/m^3	2698
melting point, °C	660.2
boiling point, °C	2494
thermal conductivity at 25 °C, W/(m·K)	234.3
latent heat of fusion, J/g[a]	395
latent heat of vaporization at bp, ΔH_v, kJ/g[a]	10,777
electrical conductivity	65% IACS[b]
electrical resistivity at 20°C, Ω·m	2.6548×10^{-8}
temperature coefficient of electrical resistivity, Ω·m/°C	0.0043
electrochemical equivalent, mg/°C	0.0932
electrode potential, V	-1.66
magnetic susceptibility, g^{-1}	0.6276×10^{-6}
Young's modulus, MPa[c]	65,000
tensile strength, MPa[c]	50

[a]To convert J to cal, divide by 4.184.

[b]International Annealed Copper Standard.

[c]To convert MPa to psi, multiply by 145.

3.1.1 Aluminium oxides or Alumina (Al_2O_3)

Aluminum oxides, which are a term of alumina compounds, had transition phase and alpha phase alumina.

- Transition alumina

The partial dehydration of aluminum hydroxides and oxyhydroxides leads to compounds with the crude formula $Al_2O_3 \times H_2O$ with $0<x<1$, which generally are poorly crystallized. These compounds are used to apply as catalyst supports, claus catalysts, and adsorbents. There are six principle phases designated by the Greek letters chi, kappa, eta, theta, delta, and gamma. The nature of the product obtained by calcination depends on the starting hydroxide (Gibbsite, boehmite and others) and on the calcination conditions. In effect, there exist several sequences during dehydration. In all cases, the ultimate product of dehydration is corundum (Al_2O_3). An excellent bibliographical review of transition alumina has been complied by Leonard (1967).

The situation can be reduced to a sample one on the basis of crystallographics, once one becomes aware that there are only two types of structures: spinel, for eta, gamma, delta, and theta and hexagonal, for chi and kappa.

3.1.2 Aluminate

A negative ion are usually given the formula AlO_2^- and derived from aluminum hydroxide. Solutions of aluminates are strongly basic.

3.2 Cobalt [42]

Cobalt, a transition series metallic element having atomic number 27, is similar to silver in appearance.

Cobalt and cobalt compounds have expanded from use as colorants in glasses and ground coat frits for pottery to drying agents in paints and lacquers, animal and human nutrients, electroplating materials, high temperature alloys, hard facing alloys, high speed tools, magnetic alloys, alloys used for prosthetics, and uses in radiology. Cobalt is also used as a catalyst for hydrocarbon refining from crude oil for the synthesis of heating fuels.

- Physical properties

The electronic structure of cobalt is [Ar] $3d^7 4s^2$. At room temperature the crystalline structure of the α (or ϵ) form, is close-paced hexagonal (cph) and lattice parameters are a = 0.2501 nm and c = 0.4066 nm. Above approximately 417°C, a face-centered cubic (fcc) allotrope, the γ (or β) form, having a lattice parameter a = 0.3544 nm, becomes the stable crystalline form. Physical properties of cobalt are listed in Table 3.2.

The scale formed on unalloyed cobalt during exposure to air or oxygen at high temperature is double-layered. In the range of 300 to 900°C, the scale consists of a thin layer of mixed cobalt oxide, Co_3O_4, on the outside and cobalt (II) oxide, CoO, layer next to metal. Cobalt (III) oxide, Co_2O_3, may be formed at temperatures below 300°C. Above 900°C, Co_3O_4 decomposes and both layers, although of different appearance, are composed of CoO only. Scales formed below 600°C and above 750°C appear to be stable to cracking on cooling, whereas those produced at 600-750°C crack and flake off the surface.

Cobalt forms numerous compounds and complexes of industrial importance. Cobalt, at wt 58.933, is one of the three members of the first transition series of Group 9 (VIIIB). There are thirteen know isotopes, but only three are significant: ^{59}Co is the

only stable and naturally occurring isotope; ^{60}Co has a half-life of 5.3 years and is a common source of γ-radioactivity; and ^{57}Co has a 270-d half-life and provides the γ-source for Mössbauer spectroscopy.

Cobalt exists in the +2 or +3 valance states for the majority of its compounds and complexes. A multitude of complexes of the cobalt (III) ion exists, but few stable simple salts are known. Octahedral stereochemistries are the most common for cobalt (II) ion as well as for cobalt (III). Cobalt (II) forms numerous simple compounds and complexes, most of which are octahedral or tetrahedral in nature; cobalt (II) forms more tetrahedral complex than other transition-metal ions. Because of the small stability difference between octahedral and tetrahedral complexes of cobalt (II), both can be found equilibrium for a number of complexes. Typically, octahedral cobalt (II) salts and complexes are pink to brownish red; most of the tetrahedral Co (II) species are blue.

Table 3.2 Physical properties of cobalt

Property	Value
atomic number	27
atomic weight	58.93
transformation temperature, °C	417
heat of transformation, J/g[a]	251
melting point, °C	1493
latent heat of fusion, ΔH_{fus} J/g[a]	395
boiling point, °C	3100
latent heat of vaporization at bp, ΔH_{vap}, kJ/g[a]	6276
specific heat, J/(g·°C)[a]	
15-100 °C	0.442
molten metal	0.560
coefficient of thermal expansion, $°C^{-1}$	
cph at room temperature	12.5
fcc at 417°C	14.2
thermal conductivity at 25 °C, W/(m·K)	69.16
thermal neutron absorption, Bohr atom	34.8
resistivity, at 20°C[b], Ω·m	6.24×10^{-8}
Curie temperature, °C	1121
saturation induction, $4\pi I_s$, T[c]	1.870
permeability, μ	
initial	68
max	245
residual induction, T[c]	0.490
coercive force, A/m	708
Young's modulus, GPa[c]	211
Poisson's ratio	0.32

Table 3.2 Physical properties of cobalt (Cont.)

Property	Value		
hardness[f], diamond pyramid, of % Co	99.9	99.98[e]	
at 20°C	225	253	
at 300°C	141	145	
at 600°C	62	43	
at 900°C	22	17	
strength of 99.9% cobalt, MPa[g]	as cast	annealed	sintered
tensile	237	588	679
tensile yield	138	193	302
compressive	841	808	
compressive yield	291	387	

[a]To convert J to cal, divide by 4.184.

[b]Conductivity = 27.6 % of International Annealed Copper Standard.

[c]To convert T to gauss, multiply by 10^4.

[d]To convert GPa to psi, multiply by 145,000.

[e]Zone refined.

[f]Vickers.

[g]To convert MPa to psi, multiply by 145.

3.2.1 Cobalt Oxides

Cobalt (II) oxide, CoO, is an olive green, cubic crystalline material. The product of commerce is usually dark gray and contains 75-78 wt % cobalt. The simple oxide is most often produced by oxidation of the metal at temperatures above 900°C. The product must be cooled in absence of oxygen to prevent formation of Co3O4. Cobalt (II) oxide is soluble in water, ammonia solution, and organic solvents, but dissolves in strong mineral acids. It is used in glass decorating and coloring and is a precursor for the production of cobalt chemicals.

3.2.2 Cobalt aluminate ($CoAl_2O_4$)

$CoAl_2O_4$ is a binary oxide consisting of cobalt oxides and aluminum oxides that crystallize in spinel structure. The unit cell of spinels is represented by formula of AB_2O_4. The Co^{2+} ions occupy the tetrahedrally coordinated A site and Al^{3+} ions occupy the octahedrally coordinated B site. The structure of cobalt aluminate is shown in Figure 3.1

Figure 3.1 Structure of cobalt aluminate

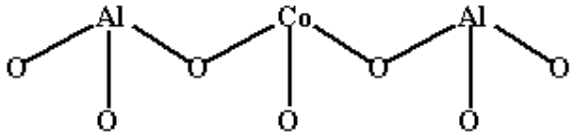

3.3 Nickel [43]

Nickel occurs in the first transition row in Group 10 (VIIIB) of the periodic table. Nickel is a high melting point element having a ductile crystal structure. Its chemical properties allow it to be combined with other elements to form many alloys.

Nickel has a [Ar] $3d^8 4s^2$ electronic configuration and forms compounds in which the nickel atom has oxidation states of -1 through +4. Whereas reagent yields an array of compounds in a variety of nickel oxidation states, Ni (II) represents the bulk of all known compounds. As of this writing, >237,000 compounds of nickel have been reported. The primary uses for nickel compounds, aside from nickel refining and electroplating, are in steel making, catalysis, storage batteries, specialty chemicals, and specialty ceramics. Some physical properties are given in Table 3.3

Table 3.3 Physical properties of nickel

Property	Value
atomic number	28
atomic weight	58.71
crystal structure	fcc
lattice constant, 25°C, nm	0.35238
melting point, °C	1453
boiling point, (by extrapolation), °C	2732
density at 20°C, g/cm^3	8.908
specific heat at 20°C,kJ/(kg·K)[a]	0.44
avg. coefficient of thermal expansion x 10^{-6}, °C^{-1}	
at 20-100°C	13.3
20-500°C	15.2
thermal conductivity, W/(m·K)	
at 100°C	82.8
300°C	63.6
500°C	61.9
electrical resistivity, at 20°C, μΩ·cm	6.97
temperature coefficient of resistivity at 0-100, (μΩ·cm)/ °C	0.0071
Curie temperature, °C	353
saturation magnetization, T[b]	0.617
residual magnetization, T[b]	0.300
coercive force, A/m[c]	239
initial permeability, mH/m[d]	0.251
max permeability, mH/m[d]	2.51-3.77
modulus of elasticity x 10^3, MPa[e]	
tension	206.0
shear	73.6
Poisson's ratio	0.30

Table 3.3 Physical properties of nickel (Cont.)

Property	Value
reflectivity, %	
at 0.30 μm	41
0.55 μm	64
3.00 μm	87
total emissivity, $\mu W/m^2$[f]	
at 20°C	45
100°C	600
500°C	120
1000°C	190
thermal neutron cross section, neutron velocity of 2200 m/s, m^2[g]	
adsorption	4.5×10^{-28}
reaction cross section	17.5×10^{-28}

[a]To convert J to cal, divide by 4.184.

[b]To convert T to G, multiply by 10^4.

[c]To convert A/m to G/Oe, divide by 79.58.

[d]To convert mH/m to G/Oe, multiply by 795.8

[e]To convert MPa to psi, multiply by 145.

[f]To convert $\mu W/m^2$ to erg/($s \cdot cm^2$), multiply by 10^{-3}.

[g]To convert m^2 to barn, divide by 1.0×10^{-28}.

3.3.1 Nickel Oxides

Nickel oxide, NiO, is a green cubic crystalline compound, mp 2090°C, density 7.45 g/cm^3, the properties of which are related to its method of preparation. Green nickel oxide is prepared by firing a mixture of water and pure nickel powder in air at 1000°C or by firing a mixture of high purity nickel powder, nickel oxide, and water in air. Whereas this temperature is required for full development of the crystal, the temperature is high enough that an equilibrium leading to dissociation back to the elements is established. Consequently, it is virtually impossible to obtain green nickel oxide made by high made by high temperature firing that does not have traces of nickel metal.

Black nickel oxide, NiO, a microcrystalline form, results from calcination of the carbonate or nitrate at 600°C. This incompletely annealed product typically has more oxygen than its formula indicates, ie, 76-77 wt % nickel compared to the green

form, which has 78.5% nickel content. This results from chemisorption of oxygen on the surface of the crystal defects. Black nickel oxide compositions are chemically reactive and form simple nickel (II) salts when heated with mineral acids. Both black and green nickel oxide can be converted to the metal by heating the carbon, carbon monoxide, or hydrogen. Both green and black nickel oxide fuse with potassium hydroxide at 700°C to form potassium nickelate, K2NiO2. Other nickel oxides, e.g., Ni_2O_3, density 4.84 g/cm^3, NiO_2, and Ni_3O_4, have been reported.

3.3.2 Nickel aluminate ($NiAl_2O_4$)

$NiAl_2O_4$ is a binary oxide consisting of nickel oxides and aluminum oxides that crystallize in spinel structure. The unit cell of spinel is represented by formula of AB_2O_4. The Ni^{2+} ions occupy the tetrahedrally coordinated A site and Al^{3+} ions occupy the octahedrally coordinated B site. The structure of nickel aluminate is shown in Figure 3.2

Figure 3.2 Structure of nickel aluminate

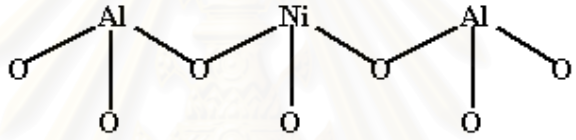

3.4 Zinc [44]

Zinc is a lustrous, blue-white metal, which can be formed into virtually any shape by the common metal-forming techniques such as rolling, drawing, extruding, etc. The hexagonal close-packed crystal structure governs the behavior of zinc during fabrication. Physical properties are given in Table 3.4

Zinc is in Group IIB of the periodic table and exhibits a valence of +2 in all its compounds. Being high on the electromotive series, zinc form quite stable compounds and, as such, resemble magnesium. Bonding in zinc compounds tends to be covalent, as in the sulfide and oxide. With strongly electropositive elements, e.g., chlorine, the bond is more ionic. The coordination number is usually four, to a lesser degree six, and in some cases five. In compounds such as the oxide, borate, and silicate, the covalent bonds with oxygen are very stable.

Table3.4 Physical properties of Zinc

Property	Value
atomic number	30
atomic weight	65.38
ionic radius, Zn^{2+}, nm	0.074
covalent radius, nm	0.131
metallic radius, nm	0.138
ionization potential, eV	
first	9.39
second	17.87
third	40.0
density	
solid, g/cm^3	
at 25°C	7.133
at 419.5°C	6.830
liquid, g/mL	
at 419.5°C	6.620
at 800°C	6.250
melting point, °C	419.5
boiling point, °C	907
heat of fusion at 419.5°C, ΔH_{fus} kJ/mol[a]	7.387
heat of vaporization at 907°C, ΔH_{vap}, kJ/mol[a]	114.8

Table3.4 Physical properties of Zinc (Cont.)

Property	Value
coefficient of thermal expansion, mm/(m·K)	
volume	8.9
linear, polycrystalline	39.7
thermal conductivity, W/(m·K)	
solid	
at 18°C	113.0
at 419.5°C	96.0
liquid	
at 419.5°C	60.7
at 750°C	56.5
electrical resistivity, nΩ/m	
polycrystalline	$R = 54.6(1+0.0042t)^b$
liquid at 423°C	369.55
heat capacity, J/(mol·K)[a]	
solid	$22.39 + 10^{-2}T^c$
liquid	31.39
gas	20.80

[a]To convert J to cal, divide by 4.184.

[b]t= 0-100°C.

[c]T= 298-692.7 K.

3.4.1 Zinc oxides

The crystal structure of zinc oxide is likely to stabilize defects, e.g., zinc excess or deficiency and inclusion of foreign ions, and therefore has useful semiconductor properties. Variously doped oxides are used for photocopying, catalysts, and phosphors.

Zinc oxide, as an amphoteric material, reacts with acids to form zinc salts and with strong alkalies to form zincates. Zinc oxide reacts with carbon dioxide in moist air to form oxycarbonate. Acidic gases, e.g., hydrogen sulfide, sulfur dioxide, and chlorine, react with zinc oxide, and carbon monoxide or hydrogen reduce it to metal.

3.4.2 Zinc aluminate ($ZnAl_2O_4$)

$ZnAl_2O_4$ is a binary oxide consisting of zinc oxides and aluminum oxides that crystallize in spinel structure. The unit cell of spinels is represented by formula of AB_2O_4.

The Zn^{2+} ions occupy the tetrahedrally coordinated A site and Al^{3+} ions occupy the octahedrally coordinated B site. The structure of zinc aluminate is shown in Figure 3.3

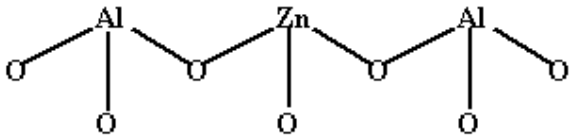

Figure 3.3 Structure of zinc aluminate

3.5 Metal alkoxides [45]

Metal alkoxides are compounds in which a metal is attached to one or more alkyl groups by an oxygen atom (Figure 3.4). Alkoixdes are derived from alcohols by the replacement of the hydroxyl hydrogen by metal.

Sodium ethoxide was the first metal alkoxide described by J. Liebig in 1837. The alkoxides of many transition metals were developed after World War II, especially by Bradley and also by Mehrotra. Today some alkoxides, including those of sodium, potassium, magnesium, aluminum, zirconium, and titanium, are commercially important. The name metal alkoxide is preferred, although metal alcoholates is also used.

Alkoxides of nonmetals can be found under the corresponding compounds, e.g., Boron or Silicon compounds. Metal alkyls, in which the alkyl group is bound directly to the metal, are discussed under the corresponding elements, e.g., Aluminum compounds and Organometallics.

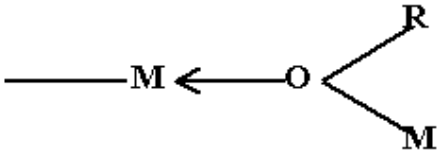

Figure 3.4 The structure of metal oxide.

- Physical properties

The metal alkoxides exhibit great differences in physical properties, depending on the position of the metal in the periodic table, and secondarily on the alkyl group. Many alkoxides are strongly associated by intermolecular forces, which depend on the size and shape of the alkyl groups.

Many metal alkoxides are soluble in the corresponding alcohols, but magnesium alkoixdes are practically insoluble. Only the distillable alkoxides, like those of aluminum, titanium, and zirconium amyloxides as examples.

In recent decades, Much work has been done on the structure of the metal alkoxides. The simple alkali alkoxides have an ionic lattice and a layer-like structure, but alkaline earth alkoxides show more covalent character. The aluminum alkoxides have been throughly studied and there is no doubt as to their covalent nature, the lower alkoxides are cyclic (Figure 3.5), even in solution and in the vapor phase.

Structures are highly varied among the transition metals. Metal alkoxides are colored when the corresponding metal ions are colored, otherwise not.

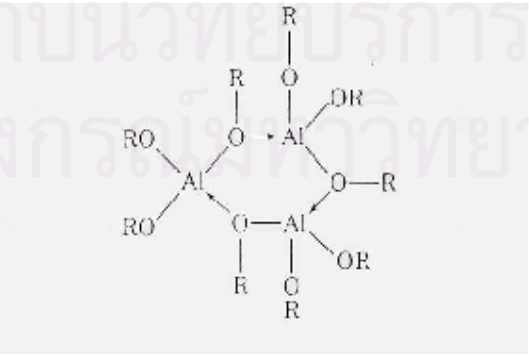

Figure 3.5 Aluminum alkoxide

- Chemical properties

The most outstanding property of the metal alkoxides is ease of hydrolysis. Uranium hexa-*tert*-butoxide is an exception and does not react with water.

3.6 Spinel [46-48]

Several of the commercially important magnetic oxides have the spinel structure. The parent spinel is $MgAl_2O_4$. It has an essentially cubic close packed array of oxide ions with Mg^{2+}, Al^{3+} in tetrahedral and octahedral interstices, respectively. There are well over a hundred compounds with the spinel structure reported to date. Most are oxides. Some are sulphides, selenides and tellurides. A few are halides. Many different cations may be introduced into the spinel structure and several different charge combinations are possible, viz.:

2, 3	as in	$MgAl_2O_4$
2, 4	as in	Mg_2TiO_4
1, 3, 4	as in	$LiAlTiO_4$
1, 3	as in	$Li_{0.5}Al_{2.5}O_4$
1, 2, 5	as in	$LiNiVO_4$
1, 6	as in	Na_2WO_4

Similar cation combinations occur with sulphides, e.g., 2, 3: $ZnAl_2S_4$ and 2, 4: Cu_2SnS_4. With halide spinels, cations are limited to charges of 1 and 2, in order to give an overall cation: anion ratio of 3:4, e.g. Li_2NiF_4.

$MgAl_2O_4$ has large, cubic unit cell with a = 8.08 Å. The cell contents are eight formula units (Z = 8) corresponding to "$Mg_8Al_{16}O_{32}$". In the *ccp* oxide array, one half of the octahedral sites is occupied by Al and one eighth of the tetrahedral sites, both T_+ and T-, by Mg.

The unit cell of the spinel structure is a large cube, eight times (i.e. 2 x 2 x 2) the size of a typical face centered cube and it is almost impossible to give a comprehensible drawing of the complete unit cell and its contents.

Writing the general formula of a normal spinel as $A^{tet}B_2{}^{oct}O_4$, let us first consider the $B_2{}^{oct}O_4$ part. Quite simply, this is the rock salt structure with *ccp* O^{2-} ions but with only alternate octahedral sites occupied by B cations. Two such rock salt-derivative subcell are shown in Figure 3.6 (a, b) (each subcell forms one octant of the spinel unit cell); the bottom face of the subcell in (a) is the same as the top face of the subcell in (b). Oxygens are shown at the corners and face centers (as in Figure 3.7).

Some octahedral positions are shown as occupied (solid circles) but alternate ones in any of the three unit cell directions are empty (small aquares).

The base of the spinel unit cell is shown (c); it is formed by the base of (b), dashed and that of three adjacent subcells. The alternating, empty-occupied-empty sequence of octahedral sites is clearly seen and also occurs similarly in the third dimension (a, b).

To complete the structure, we need to locate the tetrahedral A cations. In an *fcc* anion array, Figure 3.7, the eight tetrahedral sites, 5-12, are located as shown. These tetrahedral sites are equidistant from oxygen atoms but also from the octahedral cation sites (e.g. distances 9-A and 9-3 in Figure 3.7 are equal). Cation-cation repulsions do not allow adjacent tetrahedral and octahedral sites to be occupied simultaneously (this would be equivalent to tetrahedra and octahedral sharing a common face). We therefore need to find those tetrahedral sites for which all four neighbouring octahedral sites are empty. In Figure 3.6(a), all of the tetrahedral sites (5-12 in Figure 3.7) have at least one neighbouring octahedral cation and so none of the tetrahedral sites in this octant is occupied. The octant immediately below (or above) that in (a) is shown in (b); note that its top face is the same as the bottom face in (a). In this octant, two of the tetrahedral sites (positions 8 and 9 in Figure 3.7) have no octahedral cation neighbours and therefore, both of those contain an A cation. Taking the spinel structure as a whole, the eight octants fall into two structure groups, as represented by (a) and (b). The A cations are located in the four octants of type (b).

The two types of octant are arranged such that they alternate in any of the three unit cell directions. They are, in fact, arranged in exactly the same way as anions and cations in the rock salt structure, Figure 3.6(d). A projection of the unit cell onto one face, showing cation positions only, is show in (e). The orientation is exactly the same as in (b) and (c) but now atom heights, above the plane of the paper, are given as multiples of *c*/8. Octahedral positions are solid circles, occupied tetrahedral positions are represented by A. Octahedral atoms O' in the base (height O) are the same as in (b, c).

We have given here a simplified description of the spinel structure. In practice, the anions are displaced slightly from their corner and face center positions. The degree of displacement varies slightly from compound to compound which does mean that the bond lengths to A and B cations can change so as to best fit those required by the particular A and B ions. The origin of the spinel structure is usually shifted to

coincide with a tetrahedral A cation. We need not pursue this any further as it may lead to confusion, but it does lead to alternative descriptions of the spinel structure (e.g. the A cations alone are arranged in the same way as the C atoms in the diamond structure).

A complicating factor in some spinel structures is that the cation distribution may vary. Two extreme types of behavior may be distinguished. In normal spinels, the cations occupy sites given by the formula.

$$[A]^{tet}[B_2]^{oct}O_4$$

i.e., with A in tetrahedral sites and B in octahedral sites. Examples of normal spinels are $MgAl_2O_4$ and $MgTi_2O_4$. In inverse spinels, half of B ions occupy tetrahedral sites, leaving the remaining B ions and all the A ions in octahedral sites, i.e.

$$[B]^{tet}[A,B]^{oct}O_4$$

Usually the cations A and B are disordered over the octahedral sites. Examples of inverse spinels are $MgFe_2O_4$ and $MgTiO_4$.

As well as normal and inverse spinels, a complete range of intermediate cation distributions is possible and in some cases, the distribution changes with temperature. The cation distribution may be quantified using a parameter, γ, which is the fraction of A ions o the octahedral sites:

Normal:	$[A]^{tet}[B_2]^{oct}O_4$	$\gamma = 0$
Inverse:	$[B]^{tet}[A,B]^{oct}O_4$	$\gamma = 1$
Random:	$[B_{0.67}A_{0.33}]^{tet}[A_{0.67}B_{1.33}]^{oct}O_4$	$\gamma = 0.67$

The cation distribution in spinels and the degree of inversion, γ, have been studied in considerable detail. Several factors influence γ, including the site preferences of ions in terms of size, covalent bonding effects and crystal field stabilization energies. The γ value in any particular spinel is given by the net effect of these various parameters taken together. Some compounds with the spinel structure are given in Table 3.5

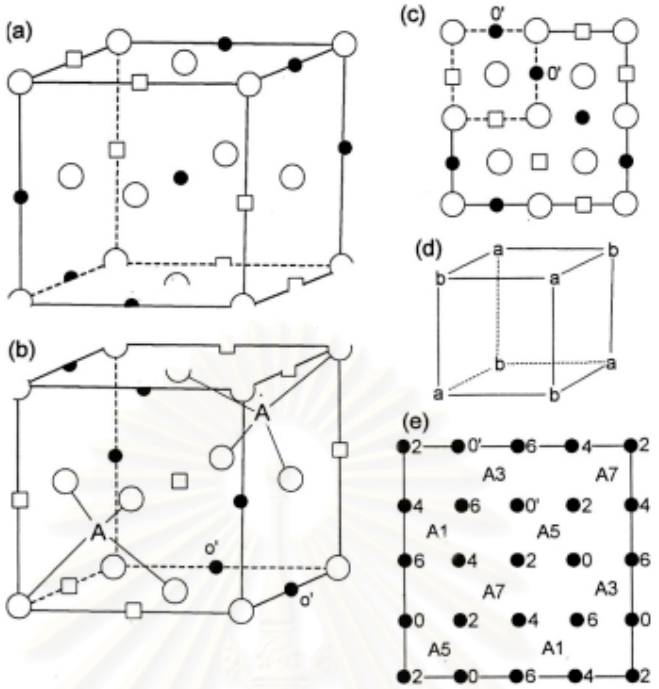

Figure 3.6 Representative parts of the spinel structure. (a) One octant of the unit cell showing oxygens at corner and face centers, empty □ and occupied (•) octahedral sites. (b) A second octant, underneath the one in (a) showing in addition the occupation of two tetrahedral sites, A. (c) One face of the cubic unit cell of the spinel structure. The dashed part coincides with the base of the subcell shown in (b). (d) Alternating arrangement of two types of octant (a) and (b). (e) Cation positions in spinel. Numbers refer to fractional heights, as multiples of *c*/8. Oxygens O' are also shown in (b, c).

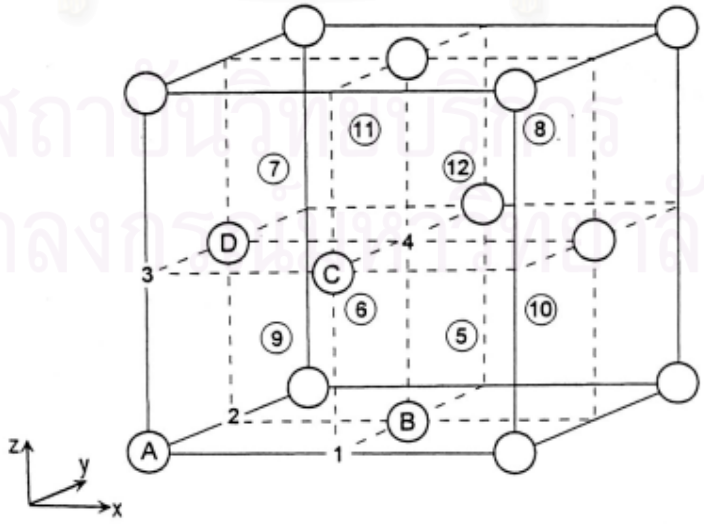

Figure 3.7 Available cation sites, 1-12, in an *fcc* anion array

Table 3.5 Some compounds with the spinel structure

Compound	Type	a (Å)	Structure	Compound	Type	a (Å)	Structure
$MgAl_2O_4$	2, 3	8.0800	Normal	$MgIn_2O_4$	2, 3	8.81	Inverse
$CoAl_2O_4$	2, 3	8.1068	Normal	$MgIn_2S_4$	2, 3	10.708	Inverse
$CuCr_2S_4$	2, 3	9.629	Normal	Mg_2TiO_4	2, 4	8.44	Inverse
$CuCr_2Se_4$	2, 3	10.357	Normal	Zn_2SnO_4	2, 4	8.70	Inverse
$CuCr_2Te_4$	2, 3	11.051	Normal	Zn_2TiO_4	1, 3, 4	8.467	Inverse
$MgTi_2O_4$	2, 3	8.474	Normal	$LiAlTiO_4$	1, 3, 4	8.34	Li in tet
Co_2GeO_4	2, 4	8.318	Normal	$LiMnTiO_4$	1, 2, 5	8.30	Li in tet
Fe_2GeO_4	2, 4	8.411	Normal	$LiZnSbO_4$	1, 2, 5	8.55	Li in tet
$MgFe_2O_4$	2, 3	8.389	Normal	$LiCoSbO_4$	1, 2, 5	8.56	Li in tet
$NiFe_2O_4$	2, 3	8.3532	Normal				

3.7 Hydrothermal methods [46-48]

Hydrothermal methods utilize water under pressure and at temperatures above its normal boiling point as means of speeding up the reactions between solids. The water performs two roles. The water-as liquid or vapour-serves as the pressure transmitting medium. In addition, some or all of the reactants to take place in, or with the aid of, liquid and/or vapour phases. Under these conditions, reactions may occur that, in the absence of water, would occur only at much higher temperatures. The method is therefore particularly suited for the synthesis of phases that are unstable at higher temperatures. It is also a useful technique for growth of single crystals; by arranging for a suitable temperature gradient to be present in the reaction vessel, dissolution of the starting material may occur at the hot end reprecipitation at the cooler end.

Since hydrothermal reactions must be carried out in closed vessels, the pressure-temperature relations of water at constant volume are importanct. These are shown in Figure 3.8. The critical temperature of water is 374°C. Below 374°C, two fluid phases, liquid and vapour, can coexist. Above 374°C only one fluid phase, supercritical water ever exists. Curve AB represents the saturated steam curve. At pressures below this curve liquid water is absent and the vapour phase is not saturated with respect to stem; on the curve the vapour is composed of saturated steam which is in equilibrium with liquid water; above the curve, liquid water is effectively under compression and the vapour phase is absent.

The dashed curves in Figure 3.8 may be used to calculate the pressure that is developed inside a vessel after it has been partially filled with water, closed and heated to a certain temperature. Thus, curve BC corresponds to a vessel that is initially 30 percent full of water: at, for example, 600°C, a pressure of 800 bar is generated inside the closed vessel. Although Figure 3.8 applied strictly to pure water, the curves are modified little, provided the solubility of solids present in the reaction vessel is small.

The design of hydrothermal equipment is basically a tube, usually of steel, closed at one end. The other end has a screw cap with a gasket of soft copper to provide a seal. Alternatively, the 'bomb' may be connected directly to an independent pressure source, such as hydraulic ram; this is known as the 'cold seal' method. The reaction mixture and an appropriate amount of water are placed inside the bomb, which is then sealed and placed inside an oven at the required temperature.

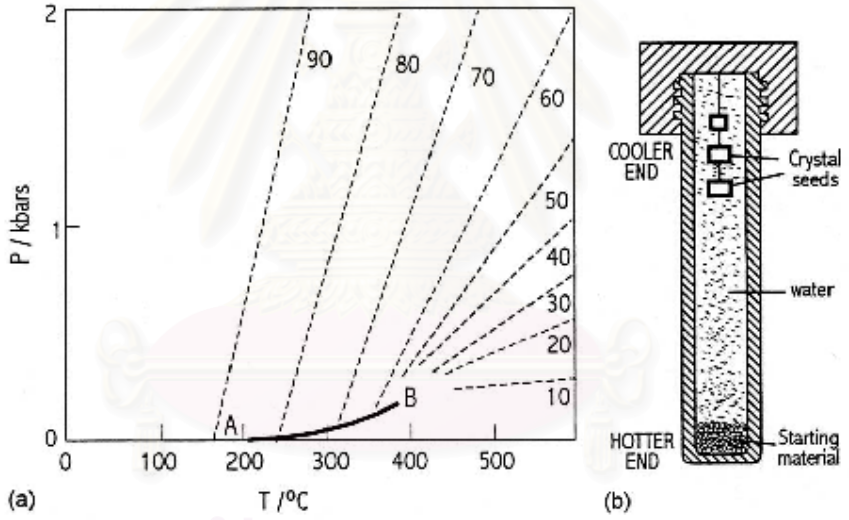

Figure 3.8 (a) Pressure-temperature relations for water at constant volume. Dashed curves represent pressures developed inside a close vessel; numbers represent the percentage degree of filling of the vessel by water at ordinary P, T. (b) Schematic hydrothermal bomb used for crystal growth.

3.7.1 Synthesis of new phases

Calcium silicate hydrates. Hydrothermal methods have been used successfully for the synthesis of many materials. A good example is the family of calcium silicate hydrates, many of which are important compounds of set cement and concrete. Typically, lime, CaO and quartz, SiO_2, are heated with water at temperature in the 150 to 500°C and pressure of 0.1 to 2.0 kbar. Each calcium silicate hydrate has, for its

synthesis, optimum preferred conditions of composition of starting mix, temperature, pressure and time. For example, xonotlite, $Ca_6Si_6O_{17}(OH)_2$, may be preheated by heating equimolar mixtures of CaO and SiO_2 at saturated steam pressures in the range 150 to 350°C, by varying the experimental conditions, H.F.W. Taylor and others have been able to unravel the chemistry of this complex family of solids.

3.17.2 Growth of single crystals

For the growth of single crystals by hydrothermal methods it is often necessary to add a mineralizer. A mineralizer is any compound added to the aqueous solution that speeds up its crystallization. It usually operates by increasing the solubility of the solute through the formation of soluble species that would not usually be in the water. For instance, the solubility of quartz in water at 400°C and 2 kbar is too small to permit the recrystallization of quartz, in a temperature gradient, within a reasonable space of time. On addition of NaOH as a mineralizer, however, large quartz crystals may be readily grown. Using the following condition, crystals of kilogram size have been grown: quartz and 1.0 M NaOH solution are held at 400°C and 1.7 kbar; at this temperature some of the quartz dissolves. A temperture gradient is arranged to exist in the reaction vessel and at 360°C the solution is supersaturated with respect to quartz, which precipitates onto a seed crystal. In summary, therefore quartz dissolves in the hottest part of the reaction vessel, is transported throughout the vessel via convection currents and it precipitated in cooler parts of the vessel where its solubility in water is lower. Quartz single crystals are used in many devices in radar and sonar, as piezoelectric transducers, as monochromators in X-ray diffraction, etc. Annual world production of quartz single crystal, using hydrothermal and other methods, is currently is currently a staggering 600 tons!

Using similar methods, many substances have been prepared as high quality single crystals, e.g. corundum (Al_2O_3) and ruby (Al_2O_3 doped with Cr^{3+}).

EXPERIMENTAL

The experimental system and procedures in the synthesis of spinels ($CoAl_2O_4$, $ZnAl_2O_4$ and $NiAl_2O_4$) are presented in this chapter. The chemicals and experimental equipments are shown in sections 4.1 and 4.2, respectively. In sections 4.3, the catalyst preparation and characterization are explained.

4.1 Chemicals

The synthesis of spinels is prepared with the following reagents:

1. Aluminium Isopropoxide (AIP, $[(CH_3)_2CHO]_3Al$) available from Aldrich, 98%+
2. Cobalt(II) acetylacetonate $[CH_3COCH=C(O-)CH_3]_2Co$ available from Aldrich,97%
3. Zinc(II) acetylacetonate $[CH_3COCH=C(O-)CH_3]_2Zn$ available from Merck, 95%+
4. Nickel(II) acetylacetonate $[CH_3COCH=C(O-)CH_3]_2Ni$ available from Aldrich, 95%
5. Toluene ($C_6H_5CH_3$) available from Carlo Erba Reagenti, 99.5%

Table 4.1 Reagents used for synthesis of spinels

Reagents	Weight/Volume
For Cobalt aluminate ($CoAl_2O_4$), Co/Al = 0.5	
Cobalt (II) acetylacetonate	9.4425 g
Aluminum isopropoxide	15 g
Zinc aluminate ($ZnAl_2O_4$), Zn/Al = 0.5	
Zinc (II) acetylacetonate	9.4339 g
Aluminum isopropoxide	15 g
Nickel aluminate ($NiAl_2O_4$), Ni/Al = 0.5	
Nickel (II) acetylacetonate	9.6791 g
Aluminum isopropoxide	15 g

The calculation of the amount of reagents used is shown in **APPENDIX A**.

Each synthesis used toluene as a solvent

in the synthesis mixture	100 cm^3
in the gap	40 cm^3

4.2 Equipment

The equipment for the synthesis of spinels and metal oxides consisted of:

4.2.1 Autoclave reactor

- Made from stainless steel
- 1000 cm^3 volume
- 10 cm inside diameter
- Pressure gauge within the range of 0 – 140 bar
- Relief valve used to control pressure in the autoclave
- Iron jacket was used to reduce the volume of autoclave to be 300 mL
- Beakers were used to contain the reactant and collect the fluid separated from super critical drying made of glass with 3-mm thickness.

Autoclave can be operated high temperature and pressure. The reaction was carried out under autogeneous pressure, which gradually increased as the temperature was raised.

The components of autoclave reactor are shown in Figure 4.1

4.2.2 Automatic temperature controller

- A magnetic switch connected to a variable voltage transfer
- A RKC temperature controller connected to a thermocouple with 0.5 mm diameter attached to the synthesis mixtures in the autoclave
- A dial setting established a set point at any temperature within the range 0 to 350°C

4.2.3 Electrical furnace (Heater)

Electrical furnace supplied the required heating to the autoclave for the synthesized reaction. Autoclave reactor can be operated from room temperature up to 350°C at voltage of 200 volts.

4.2.4 Gas controlling system

Nitrogen is set with a pressure regulator (0-150 bar) and needle valves are used to release gas from autoclave.

The diagram of the reaction equipment for synthesis of spinels and metal oxides is shown in Figure 4.2

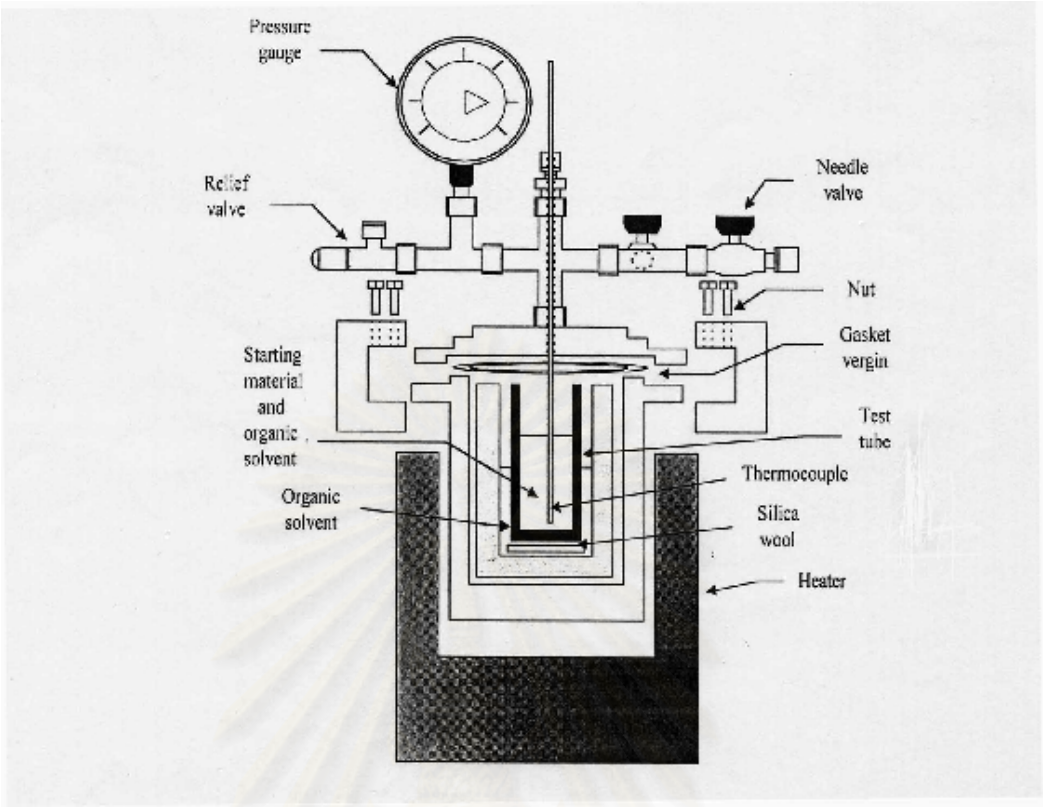

Figure 4.1 Autoclave reactor

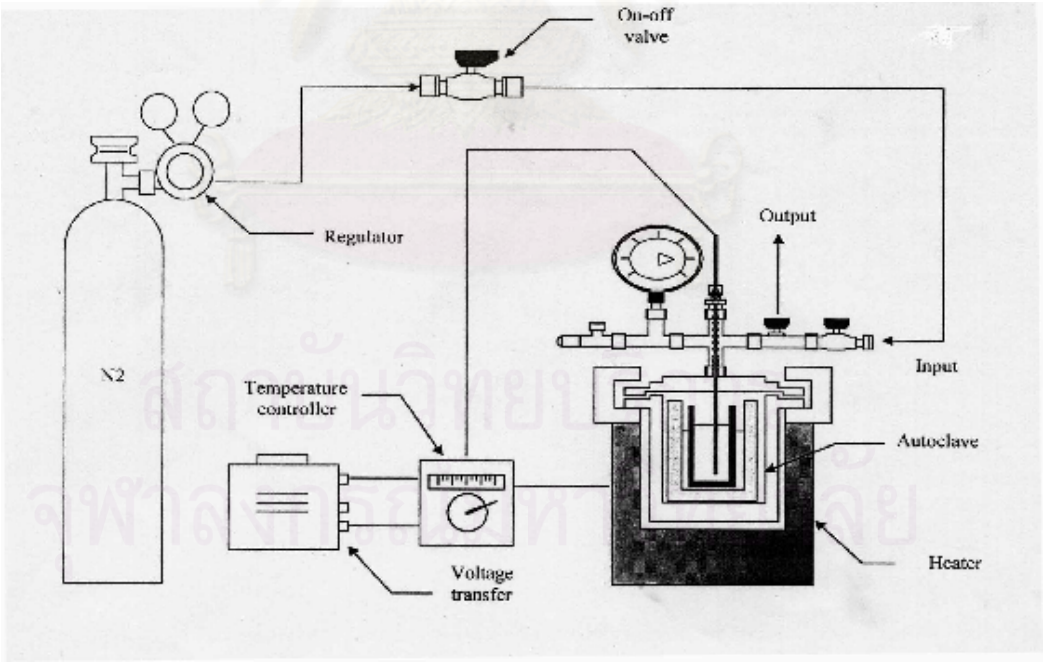

Figure 4.2 Diagram of the reaction equipment of synthesis for spinels

4.3 Preparation of spinels

$CoAl_2O_4$ was prepared by the mixture of aluminum isopropoxide, 15.0 g and appropriate amount of cobalt (II) acetylacetonate (Co/Al molar ratio = 0.5) as starting

materials while $ZnAl_2O_4$ was prepared by the mixture of aluminum isopropoxide, 15.0 g and appropriate amount of zinc (II) acetylacetonate (Zn/Al molar ratio = 0.5). Furthermore, $NiAl_2O_4$ was prepared by mixture of aluminum isopropoxide 15.0g and appropriate amount of nickel (II) acetylacetonate (Ni/Al molar ratio = 0.5). The starting materials were suspended in 100 mL of toluene in a beaker, and then set up in 300 mL autoclave. In the gap between the beaker and autoclave wall, 40 mL of toluene was added. After the autoclave was completely purged with nitrogen, the suspension was heated to 300°C at the rate of 2.5°C/min and held at that temperature for 2h. However, the same synthesis method is performed at various holding temperatures. Autogenous pressure during the reaction gradually increased as temperature was raised. Then the autoclave was cooled to room temperature. After the autoclave was cooled, the resulting products were washed repeatedly with methanol by centrifugation and dried in air. The calcination of the thus-obtained product carried out in a furnace. The product was heated at a rate of 10°C/min to a desired temperature (500, 600, 800, 900 and 1000°C) and held at that temperature for 1 h.

4.4 Characterization

4.4.1 X-ray diffraction (XRD)

The X-ray diffraction (XRD) patterns of powder were recorded on a SIEMENS XRD D5000 with Ni-filtered Cu Kα radiation. Scans were performed over the 2θ ranges from 10° to 80° for spinels. The crystallite size was estimated from line broadening according to the Scherrer equation. The value of shape factor, K was taken to be 0.9 and α-Al_2O_3 was used to be internal standard.

4.4.2 Morphology

The morphology and crystallite size of the samples were observed by a JEOL TEM-200cx Transmission Electron Microscope at the Scientific and Technological Research Equipment Center, Chulalongkorn University (STREC).

4.4.3 BET Apparatus

The BET surface areas were calculation by the Brunauer-Emmett-Teller single point method on the basis of the nitrogen uptake measured (P/P_0= 0.3) at liquid-nitrogen boiling point temperature equipped with using a gas chromatograph.

The apparatus consisted of two gases feed lines for helium and nitrogen. The fine-metering valve was used to adjust the flow rate of gas. The sample cell made

from pyrex glass. The operation conditions of gas chromatograph (GOW-MAC) are shown in Table 4.2.

Table 4.2 The operation conditions of gas chromatograph (GOW-MAC)

Model	**GOW-MAC**
Detector	TCD
Helium flow rate	30 mL/min
Detector temperature	80°C
Detector current	80 mA

The mixture of helium and nitrogen gas flowed through the system at nitrogen relative pressure of 0.3. The sample was placed in the sample cell. Then it was heated up to 150°C and held at this temperature for 2 h. The sample was cooled down to room temperature and ready to measure the surface area. There are three steps for measuring the BET surface area such as:

1. Adsorption step

The sample cell, which in had desired measuring sample, was dipped into the liquid nitrogen. Nitrogen gas was adsorbed on the surface of the sample until equilibrium was reached.

2. Desorption step

The nitrogen-adsorbed sample, which was in the sample cell, was dipped into the water at room temperature. The adsorbed nitrogen was desorbed from the surface of the sample. This step was completed when the recorder line became to the base line.

3. Calibration step

1 mL of nitrogen at atmospheric pressure was injected at the calibration port. Then the area, which was calibration peak, was measured.

Sample of calculation of the BET surface area is shown in **APPENDIX B**.

RESULTS AND DISCUSSION

In this study, the transition metals of the first series in the Periodic Table, which were scandium (Sc), titanium (Ti), vanadium (V), chromium (Cr), manganese (Mn), iron (Fe), cobalt (Co), nickel (Ni), copper (Cu) and zinc (Zn), were varied in tetrahedral site coordinations of the spinel-type structures of metal aluminate spinels. For the synthesis of metal aluminate spinels, metal (II) acetylacetonate used as a starting material such as manganese (II) acetylacetonate, cobalt (II) acetylacetonate, nickel (II) acetylacetonate, copper (II) acetylacetonate and zinc (II) acetylacetonate. Scandium, titanium, vanadium, chromium and iron were not commercial found in the form of metal (II) acetylacetonate so they were not used for this study.

The synthesis of spinels found that the manganese (II) acetylacetonate and copper (II) acetylacetonate could not be formed as the spinel-type structure of manganese aluminate ($MnAl_2O_4$) and copper aluminate ($CuAl_2O_4$), respectively. The spinel-type structure of cobalt aluminate ($CoAl_2O_4$), nickel aluminate ($NiAl_2O_4$) and zinc aluminate ($ZnAl_2O_4$) could be formed using cobalt (II) acetylacetonate, nickel (II) acetylacetonate, and zinc (II) acetylacetonate the respectively. $CoAl_2O_4$, $NiAl_2O_4$ and $ZnAl_2O_4$ spinels were formed at the reaction temperature of 300, 300 and 270°C, respectively, which the results and discussions were presented as follow:

5.1 The formation of pure cobalt aluminate ($CoAl_2O_4$)

The thermal decomposition reaction of cobalt acetylacetonate and aluminum isopropoxide with the molar ratio of Co/Al of 0.5 using toluene as a solvent at various reaction temperatures (300, 320 and 340°C) for 2h under autogeneous pressure yielded nanocrystallite cobalt aluminate ($CoAl_2O_4$). The XRD patterns of the as-synthesized products show that spinel phase was formed without contamination with other phases such as CoO, Co_3O_4 and Al_2O_3, as shown in Figure 5.1. At the reaction temperature of 290°C, the reaction in toluene could not occur as cobalt aluminate spinel. The XRD patterns of the as-synthesized products at 300°C for 2h before and after calcined at various calcination temperatures of 500, 600, 800, 900 and 1000°C are given in Figure 5.2. It shows that spinel phase did not change to other phases.

The crystallite sizes of these products calculated from the XRD line broadening ($2\theta = 37°$) were 6.50, 7.46, 7.62, 8.55, 13.22 and 22.00, respectively. The particle sizes of the as-synthesized product at 300°C before and after calcined at various calcination temperatures between 500 to 1000°C observed from the TEM photograph were close to the nanocrystallite sizes of these products calculated from the XRD line broadening. They indicated that each primary particle is a single crystal of cobalt aluminate spinel. The average particle sizes determined by using TEM and shown in Figures 5.3 (a) to 5.3 (f), were 6.33, 7.20, 7.55, 8.32, 12.93 and 22.00 nm, respectively. These were in good agreement with the crystallite sizes. The particle size data observed from the TEM photographs and XRD line broadening were shown in Table 5.1. The BET surface area of as-synthesized products at 300°C before and after calcined at various calcination temperatures of 500, 600, 800, 900 and 1000°C were 107.8, 94.94, 73.98, 38.19, 26.56 and 7.11 m^2g^{-1}, respectively, as shown in Table 5.1.

From the above results, they indicated that nanocrystallite size of products was increased with the increase of the calcination temperature. The increase of the nanocrystallite sizes of all products in the heat-treatment temperature generates grain growth by a conventional solid-state reaction, where the driving force is the decrease of total surface energies which comes about by grain contact and grain growth [8]. The BET surface area of calcined products was decreased with the increase of the calcination temperature. The increase of the reaction temperature in the synthesis condition affected the increase of the crystallite size and the decrease of the BET surface area. Then, both of the crystallite size and the BET surface area of cobalt aluminate depended on the heat treatment.

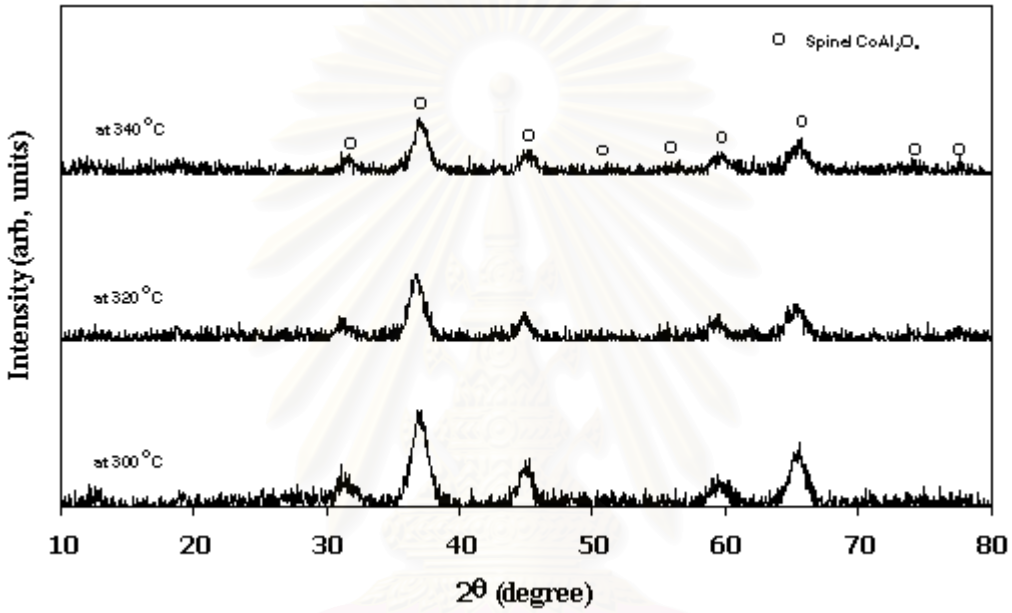

Figure 5.1 The XRD patterns of obtaining the as-synthesized cobalt aluminate spinel by the thermal decomposition reactions at various reaction temperatures equal to 300, 320 and 340°C for 2h

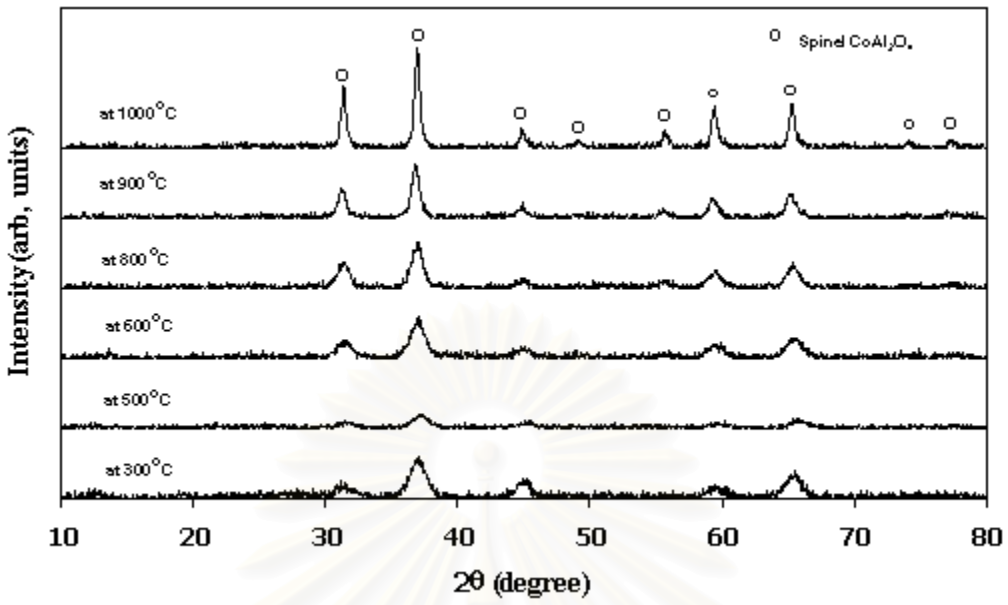

Figure 5.2 The XRD patterns of the as-synthesized cobalt aluminate spinel at 300°C for 2h before and after calcined at various calcination temperatures of 500, 600, 800, 900 and 1000°C

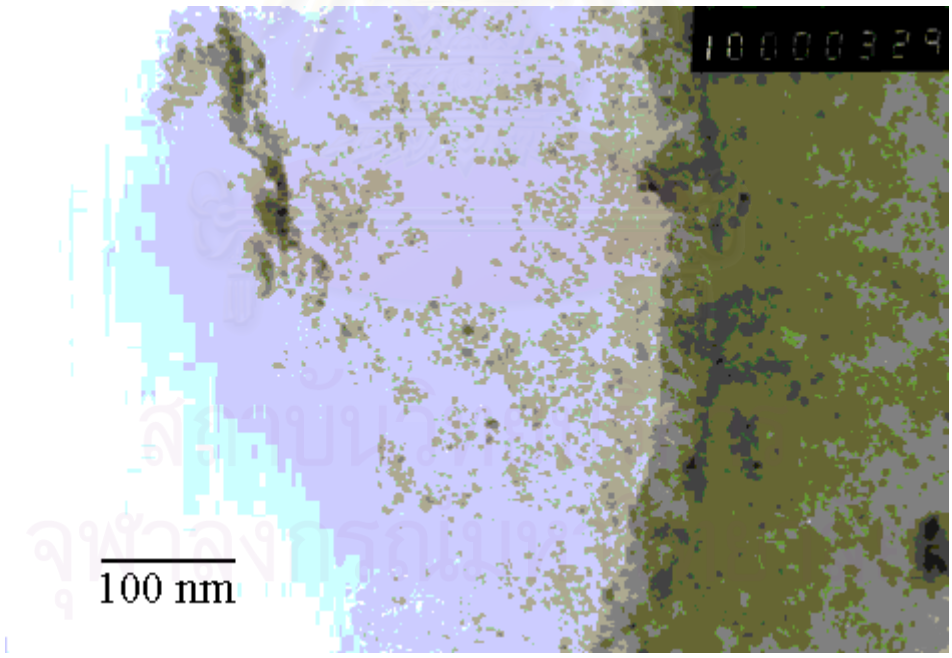

Figure 5.3 (a) TEM photograph of the as-synthesized cobalt aluminate spinel at 300°C (x150000)

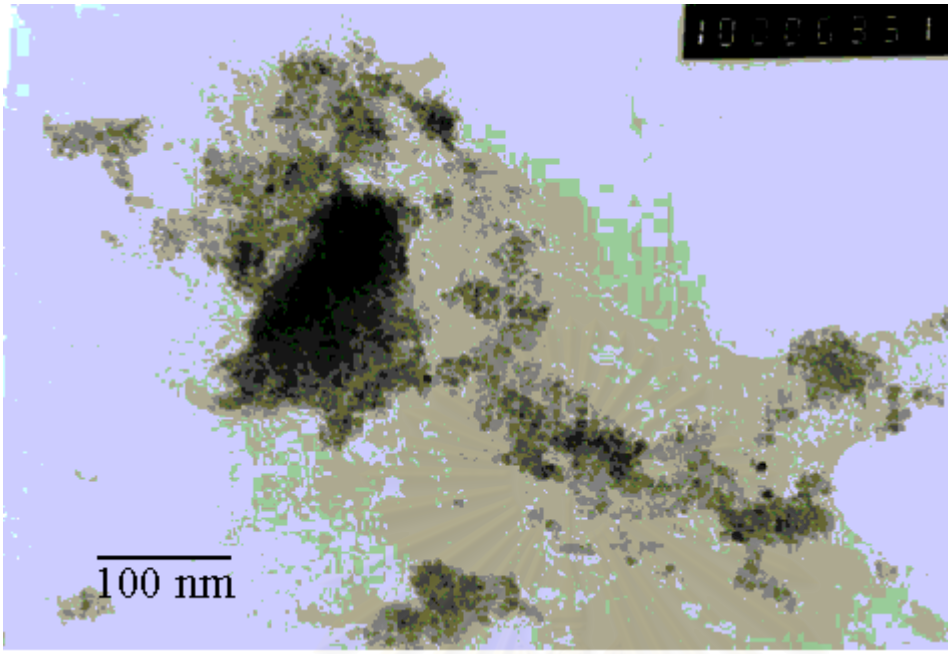

Figure 5.3 (b) TEM photograph of calcined cobalt aluminate spinel at 500°C (x150000)

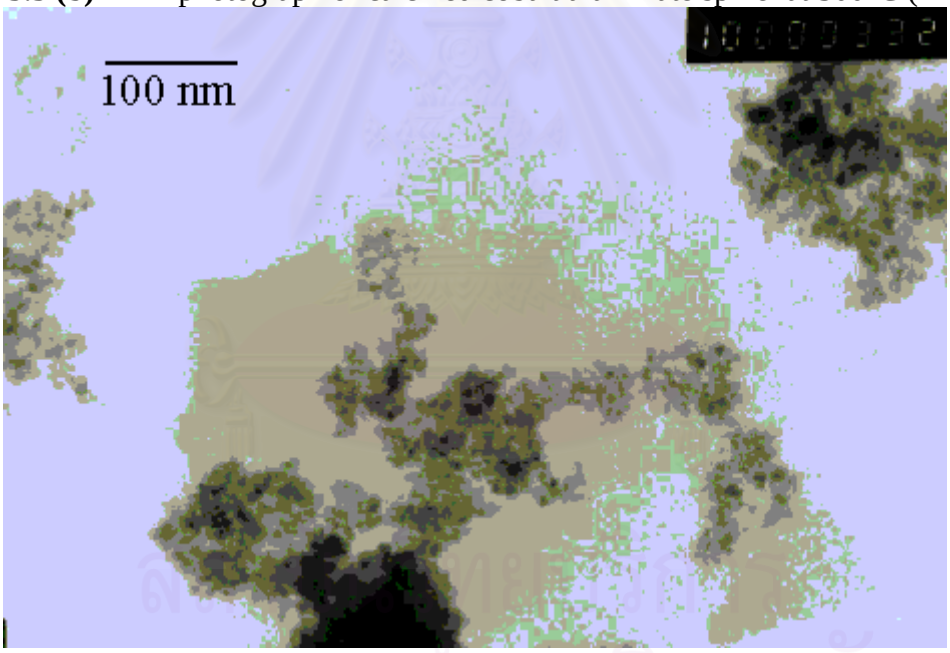

Figure 5.3 (c) TEM photograph of calcined cobalt aluminate spinel at 600°C (x150000)

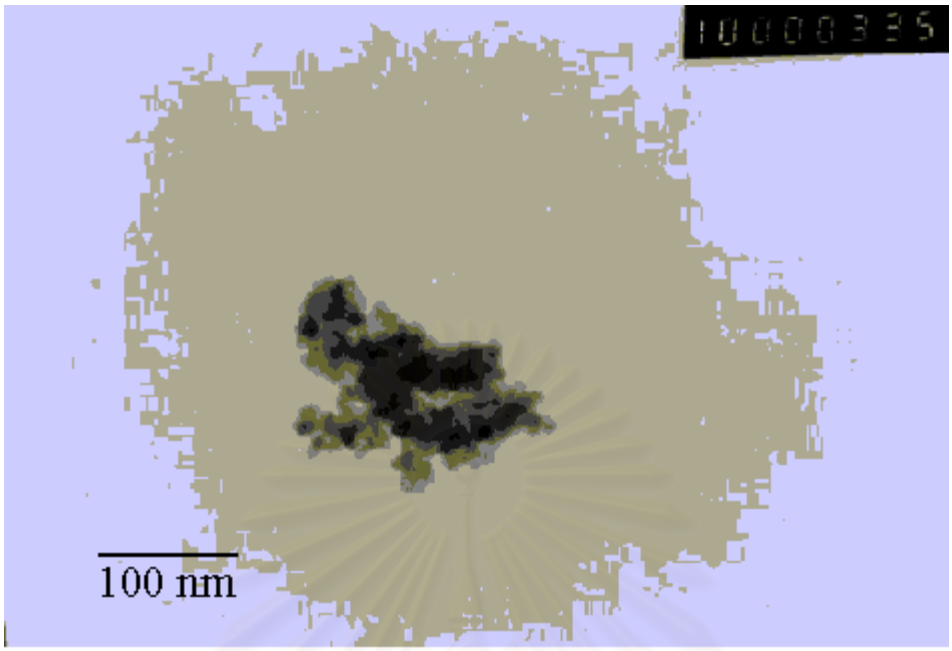

Figure 5.3 (d) TEM photograph of calcined cobalt aluminate spinel at 800°C (x150000)

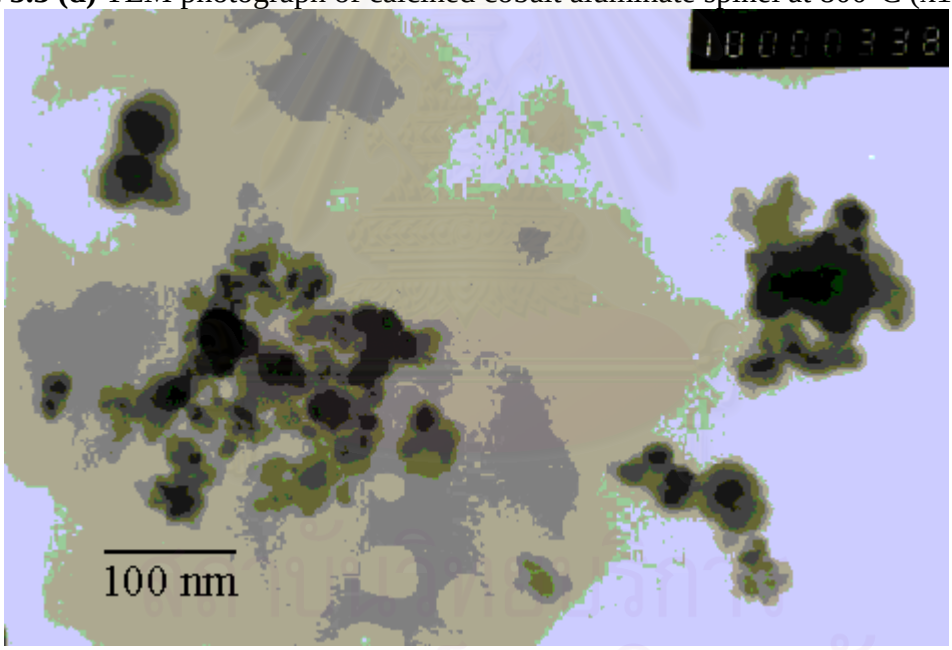

Figure 5.3 (e) TEM photograph of calcined cobalt aluminate spinel at 900°C (x150000)

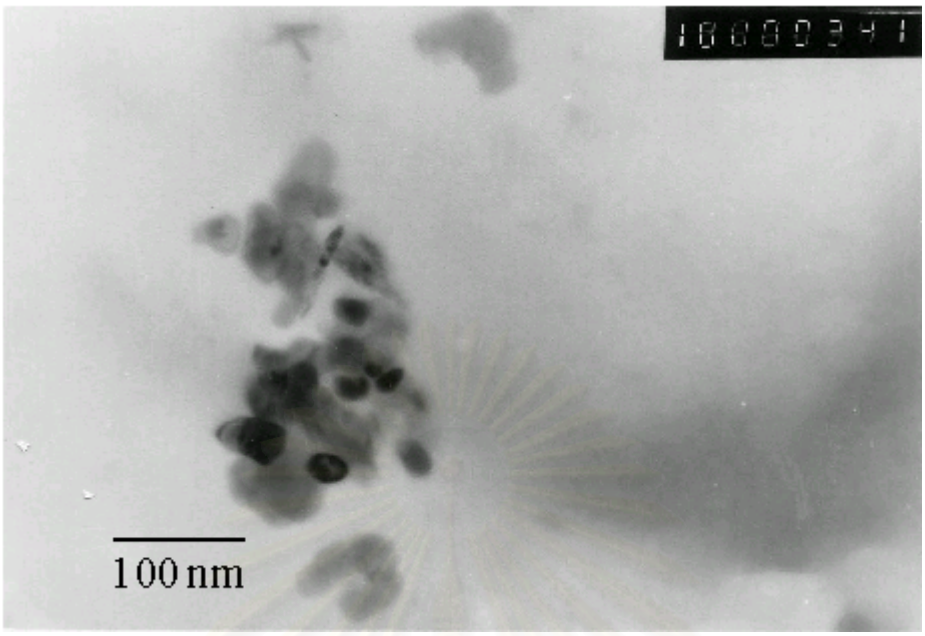

Figure 5.1.3 (f) TEM photograph of calcined cobalt aluminate spinel at 1000°C (x150000)

Table 5.1 Nanocrystallite size and the BET surface area of the as-synthesized cobalt aluminate spinel at 300°C and the calcined samples at various calcination temperatures

Sample	Calcination Temperature		Crystallite Size (nm)	Particle Size (nm)	S_{BET}[c] (m^2/g)	BET/BET_0
	T (°C)	T (K)	d^a (XRD)	d^b (TEM)		
$CoAl_2O_4$	as-syn	as-syn	6.50	6.33	107.80	-
	500	773	7.46	7.20	94.94	0.8807
	600	873	7.62	7.55	73.98	0.6863
	800	1073	8.55	8.32	38.19	0.3543
	900	1173	13.22	12.93	26.56	0.2464
	1000	1273	22.00	22.00	14.57	0.1352

[a]Crystallite size of the products calculated from Scherrer equation using α-Al_2O_3 as an internal standard.

[b]Particle size of the products calculated from TEM photograph.

[c]BET surface area

5.2 The formation of pure zinc aluminate ($ZnAl_2O_4$)

The thermal decomposition reaction of zinc acetylacetonate and aluminum isopropoxide with the molar ratio of Zn/Al of 0.5 in toluene as a solvent at various reaction temperatures of 270, 280, 290, 300 and 320°C yielded nanocrystallite zinc aluminate ($ZnAl_2O_4$). The XRD patterns of the as-synthesized products are given in Figure 5.4. It shows that the spinel phase was directly formed without other phases of zinc oxide and alumina occurred. Figure 5.5 shows the XRD patterns of the as-synthesized products at 300°C before and after calcined at the same various temperatures as the preparation of cobalt aluminate. The patterns presented the completely similar XRD characteristic peaks of the zinc aluminate spinel. At the reaction temperature of 260°C, $ZnAl_2O_4$ spinel could not be formed.

The crystallite sizes calculated from the XRD line broadening, the particle sizes measured from TEM photographs, and the BET surface area of as-synthesized products at 300°C and calcined products at various temperatures are summarized in Table 5.2. The crystallite sizes of as-synthesized products at 300°C and calcined products at 500, 600, 800, 900 and 1000°C were measured by the calculation of the XRD line broadening (2θ = 37°) as 8.33, 8.99, 11.43, 15.52, 22.91 and 33.10 nm, respectively. The TEM photographs of the as-synthesized products at 300°C before and after calcined at various temperatures are shown in Figures 5.6 (a) to 5.6 (f). The particle sizes of the as-synthesized products at 300°C and the calcined products at 500, 600, 800, 900 and 1000°C were 8.14, 8.69, 11.01, 15.50, 22.54 and 32.88 nm, respectively. The particle sizes of the products observed from the TEM photographs are in good agreement with the crystallite size determined by the XRD line broadening technique. This suggests that each particle is a single crystal of spinel.

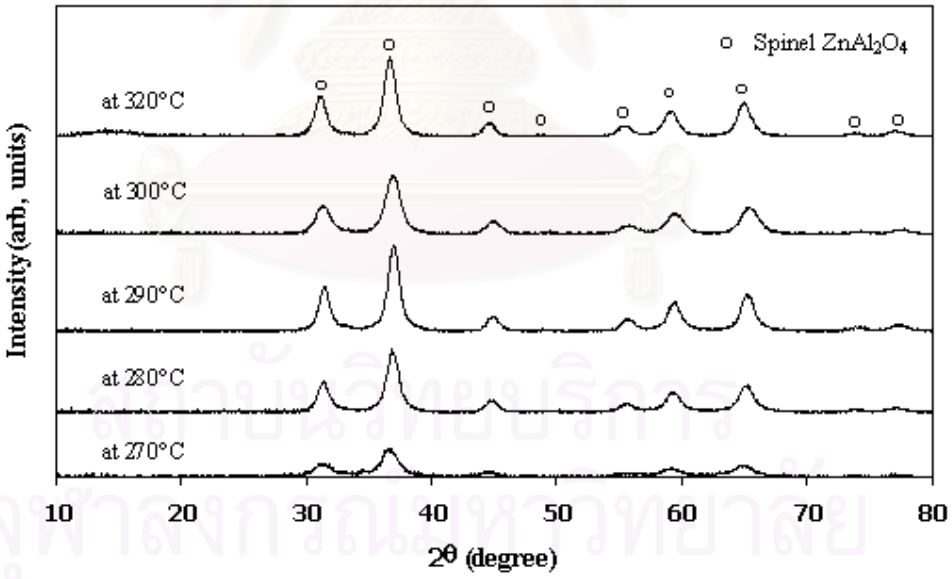

Figure 5.4 The XRD patterns of obtaining the as-synthesized zinc aluminate spinel by the thermal decomposition reaction at various reaction temperatures of 270, 280, 290, 300 and 320°C for 2h

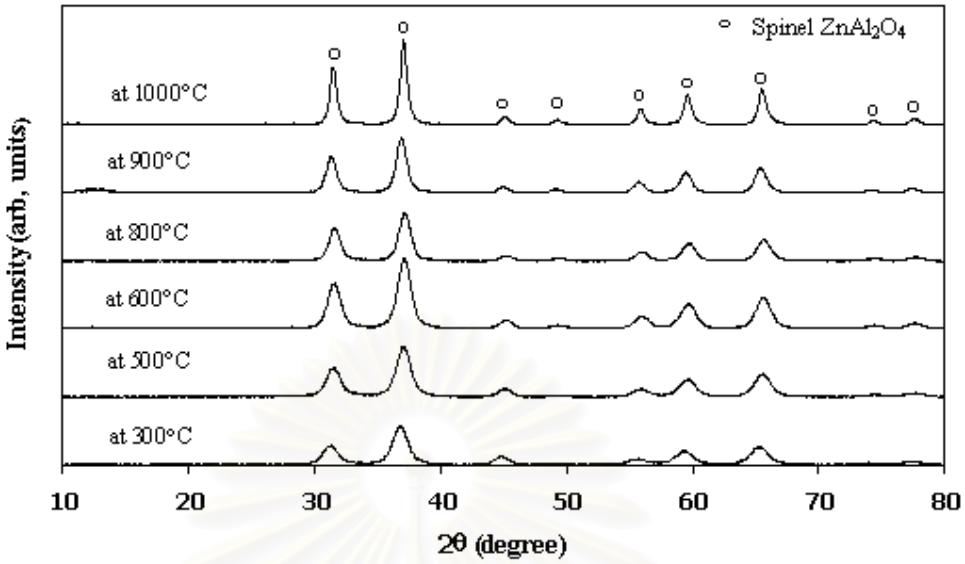

Figure 5.5 The XRD patterns of the as-synthesized zinc aluminate spinel at 300°C for 2h before and after calcined at various calcination temperatures of 500, 600, 800, 900 and 1000°C

Table 5.2 Nanocrystallite size and the BET surface area of the as-synthesized zinc aluminate spinel at 300°C and the calcined samples at various calcination temperatures

Sample	Calcination Temperature		Crystallite Size (nm)	Particle Size (nm)	S_{BET}[c] (m^2/g)	BET/BET_0
	T (°C)	T (K)	d^a (XRD)	d^b (TEM)		
$ZnAl_2O_4$	as-syn	as-syn	8.33	8.14	138.82	-
	500	773	8.99	8.69	88.00	06339
	600	873	11.43	11.01	60.31	0.4344
	800	1073	15.52	15.50	32.34	0.2330
	900	1173	22.91	22.54	19.11	0.1377
	1000	1273	33.10	32.88	9.85	0.0710

[a]Crystallite size of the products calculated from Scherrer equation using α-Al_2O_3 as an internal standard.

[b]Particle size of the products calculated from TEM photograph.

[c]BET surface area

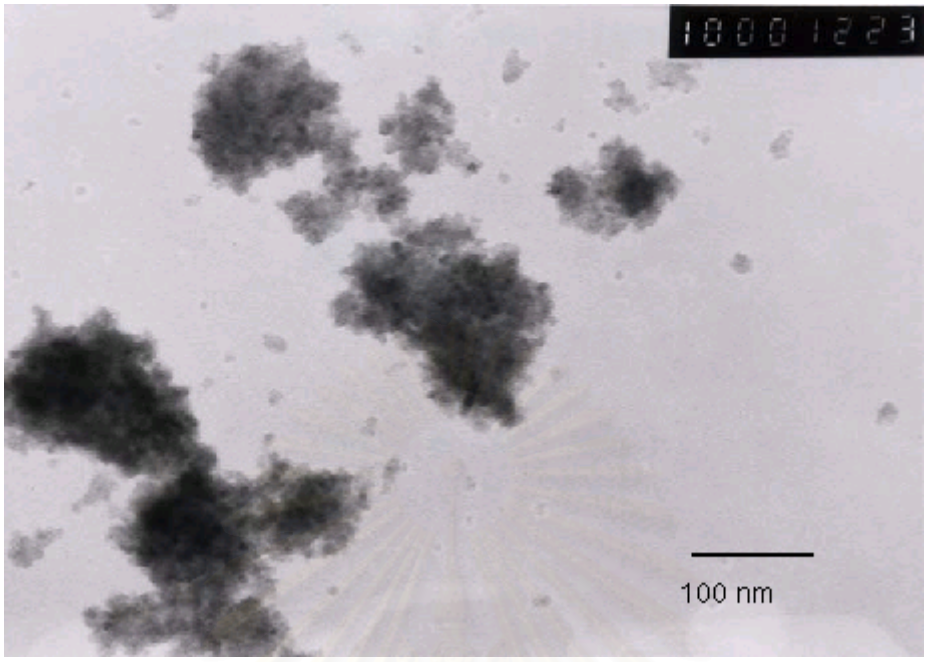

Figure 5.6 (a) TEM photograph of the as-synthesized zinc aluminate spinel at 300°C (x150000)

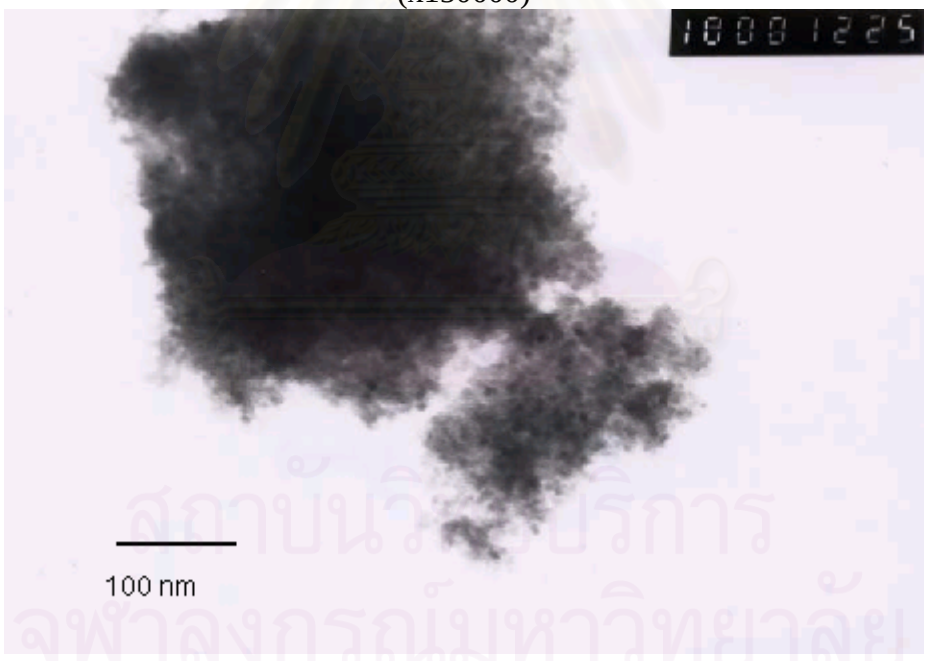

Figure 5.6 (b) TEM photograph of calcined zinc aluminate spinel at 500°C (x150000)

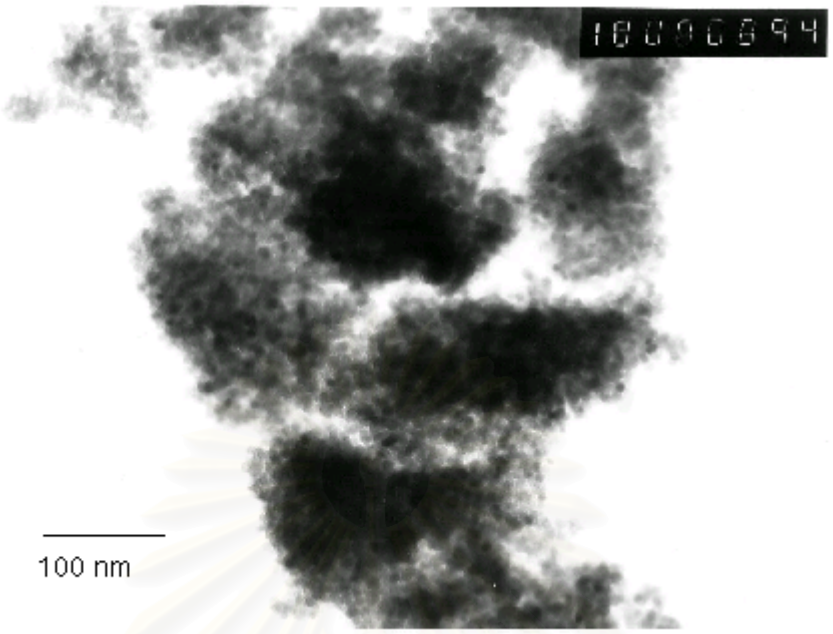

Figure 5.6 (c) TEM photograph of calcined zinc aluminate spinel at 600°C (x150000)

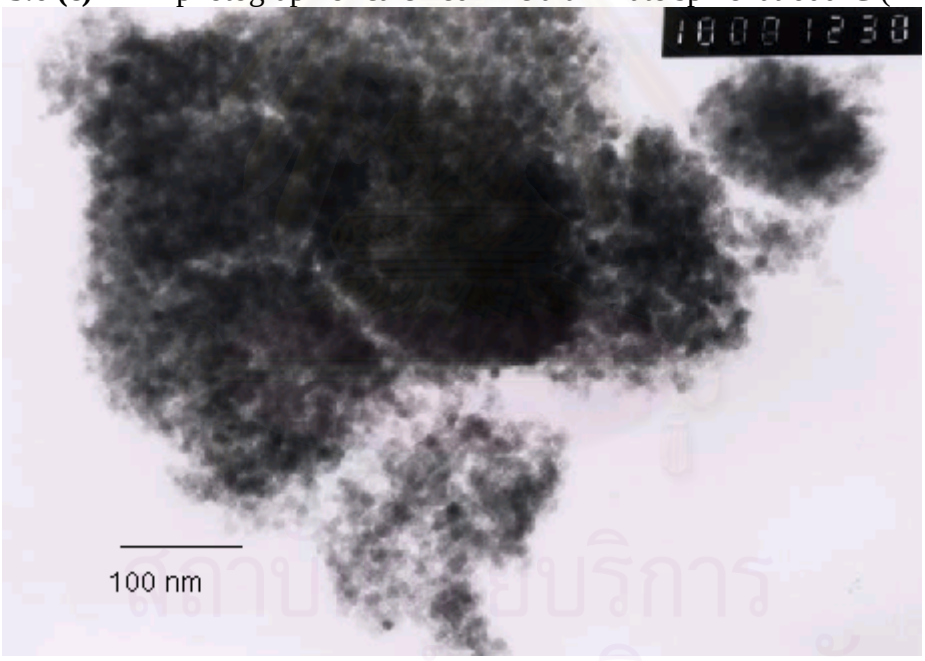

Figure 5.6 (d) TEM photograph of calcined zinc aluminate spinel at 800°C (x150000)

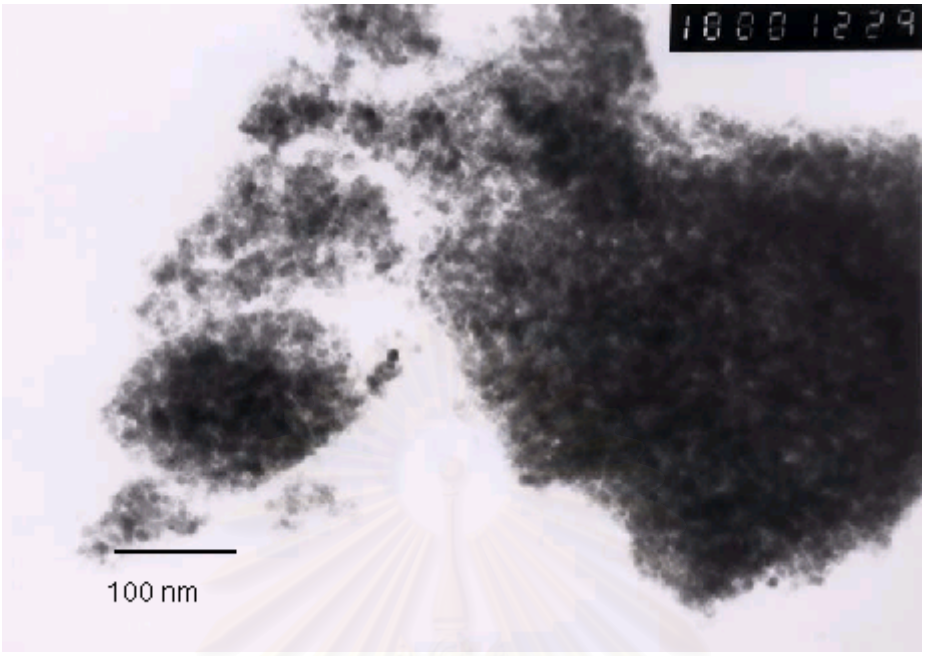

Figure 5.6 (e) TEM photograph of calcined zinc aluminate spinel at 900°C (x150000)

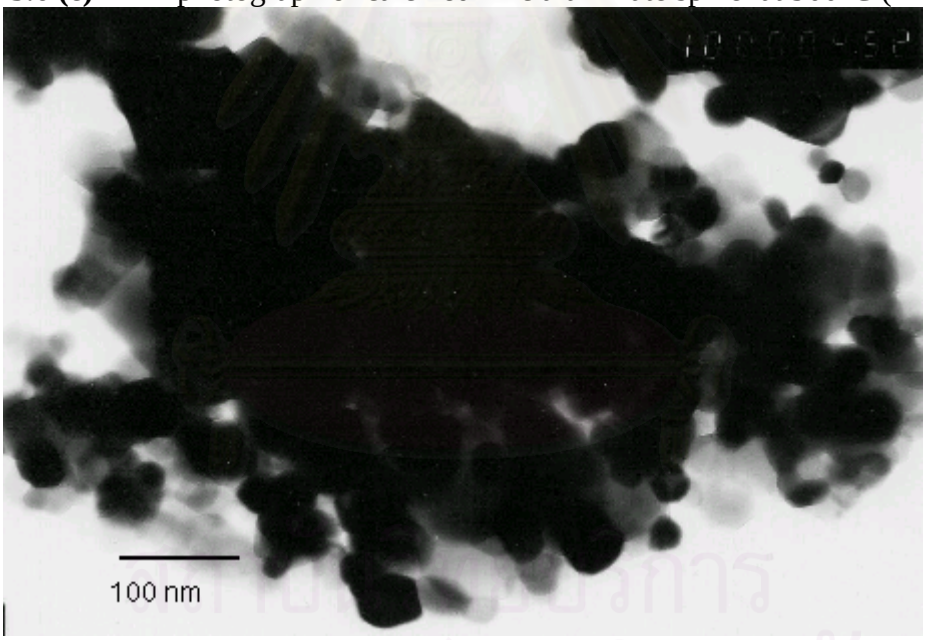

Figure 5.6 (f) TEM photograph of calcined zinc aluminate spinel at 1000°C (x150000)

The BET surface area of as-synthesized products at 300°C before and after calcined at various calcination temperatures of 500, 600, 800, 900 and 1000°C were 138.82, 88.00, 60.31, 32.34, 19.11 and 9.85 m^2g^{-1}, respectively, which was decreased with the increase of the calcination temperature. The crystallite size of the calcined products was increased with the increase of the calcination temperature. In the synthesis, the difference of the reaction temperature had effect on both of the crystallite size and the BET surface area. The increase of the reaction temperature in the synthesis condition affected the increase of the crystallite size and the decrease of the BET surface area. They indicated that the heat treatment had influence on the crystallite size and the BET surface area of $ZnAl_2O_4$ spinel. These results were the same behavior as $CoAl_2O_4$ spinel.

5.3 The formation of pure nickel aluminate ($NiAl_2O_4$)

The reaction of nickel acetylacetonate and aluminum isopropoxide in toluene solvent with the molar ratio of Ni/Al of 0.5 at the reaction temperature of 300°C, which were shown in Figure 5.7, yielded nanocrystallite nickel aluminate. The as-synthesized products were the spinel-type structure of nickel aluminate without contaminated phases such as nickel oxide and alumina. After calcined, the calcined products did not change to other phases. The XRD patterns of the as-synthesized products at 300°C and calcined products at various temperatures of 500, 600, 800, 900 and 1000°C are shown in Figure 5.7. At the reaction temperature of 290 and 320°C, $NiAl_2O_4$ spinel did not form. The products were contaminated with nickel oxides.

The crystallite sizes of $NiAl_2O_4$ spinel products before and after calcined at 500, 600, 800, 900 and 1000°C calculated by the XRD line broadening ($2\theta = 37°$) were 2.61, 3.94, 4.16, 6.09, 9.16 and 13.51 respectively, which exhibited in Table 5.3. In Figures 5.8 (a) to 5.8 (f), the TEM photograph of the as-synthesized products and calcined products at various calcination temperatures are illustrated. The particle sizes of as-synthesized products and calcined products at 500, 600, 800, 900 and 1000°C measured from the TEM photographs were 2.16, 3.51, 3.94, 6.00, 8.75 and 12.98 nm, respectively, as shown in Table 5.3. These results show good agreement with the crystallite sizes that calculated from the XRD line broadening. Then it is indicated that each particle is a single crystal.

The BET surface area of as-synthesized products at 300°C before and after calcined at various calcination temperatures of 500, 600, 800, 900 and 1000°C were 193.14, 188.54, 173.07, 121.02, 72.65 and 48.81 m^2g^{-1}, respectively, as shown in Table 5.3.

The increase of the calcination temperature affected the increase of the crystallite size and the decrease of the BET surface area as same as $CoAl_2O_4$ and $ZnAl_2O_4$ spinel products.

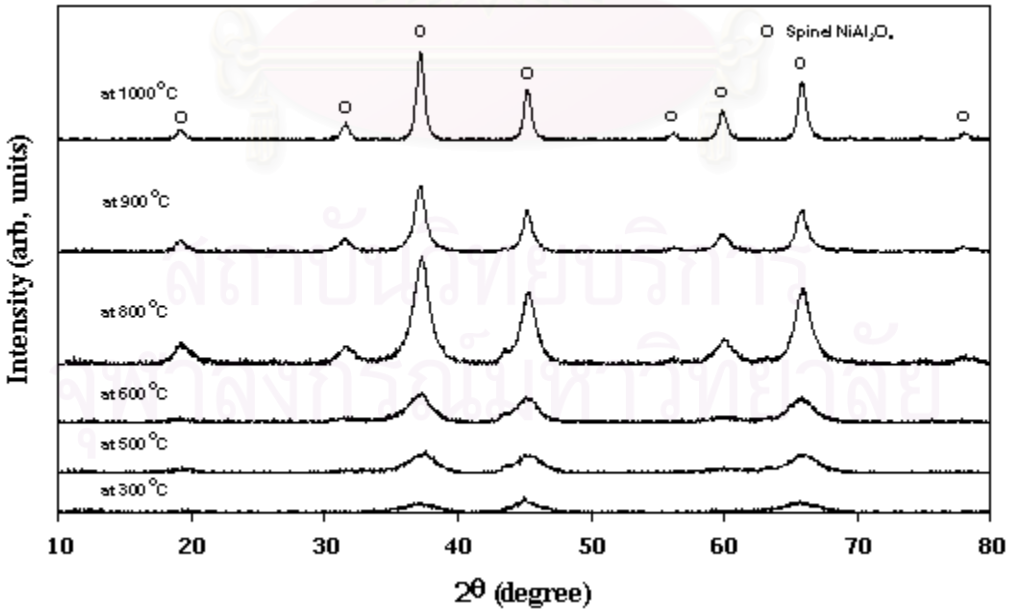

Figure 5.7 The XRD patterns of the as-synthesized nickel aluminate spinel at 300°C for 2h before and after calcined at various calcination temperatures of 500, 600, 800, 900 and 1000°C

Table 5.3 Nanocrystallite size and the BET surface area of the as-synthesized nickel aluminate spinel at 300°C and the calcined samples at various calcination temperatures

Sample	Calcination Temperature		Crystallite Size (nm)	Particle Size (nm)	S_{BET}[c] (m^2/g)	BET/BET_0
	T (°C)	T (K)	d^a (XRD)	d^b (TEM)		
$NiAl_2O_4$	as-syn	as-syn	2.61	2.16	193.14	-
	500	773	3.94	3.51	188.54	0.8807
	600	873	4.16	3.94	173.07	0.6863
	800	1073	6.09	6.00	121.02	0.3543
	900	1173	9.16	8.75	72.65	0.2464
	1000	1273	13.51	12.98	48.81	0.1352

[a]Crystallite size of the products calculated from Scherrer equation using α-Al_2O_3 as an internal standard

[b]Particle size of the products calculated from TEM photograph

[c]BET surface area

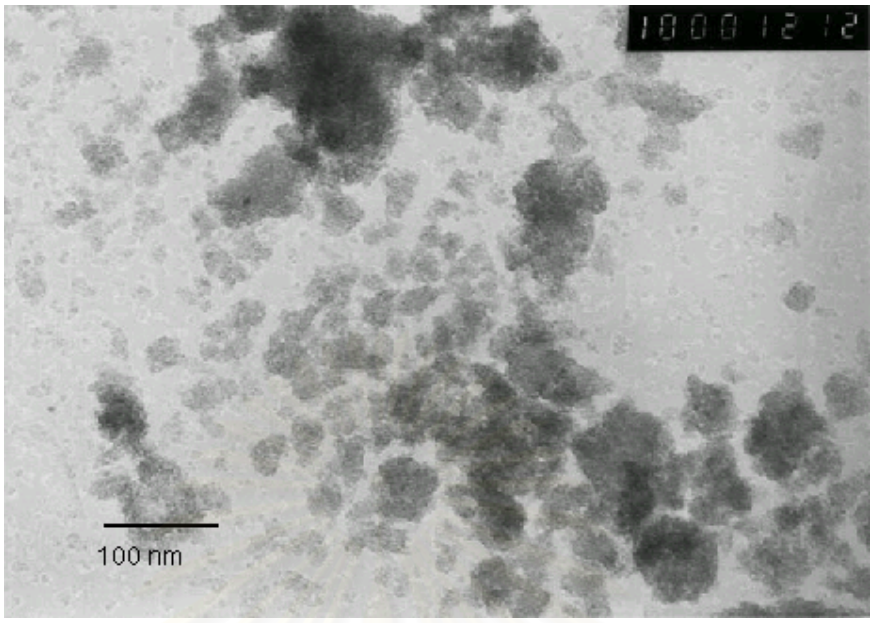

Figure 5.8 (a) TEM photograph of the as-synthesized nickel aluminate spinel at 300°C (x150000)

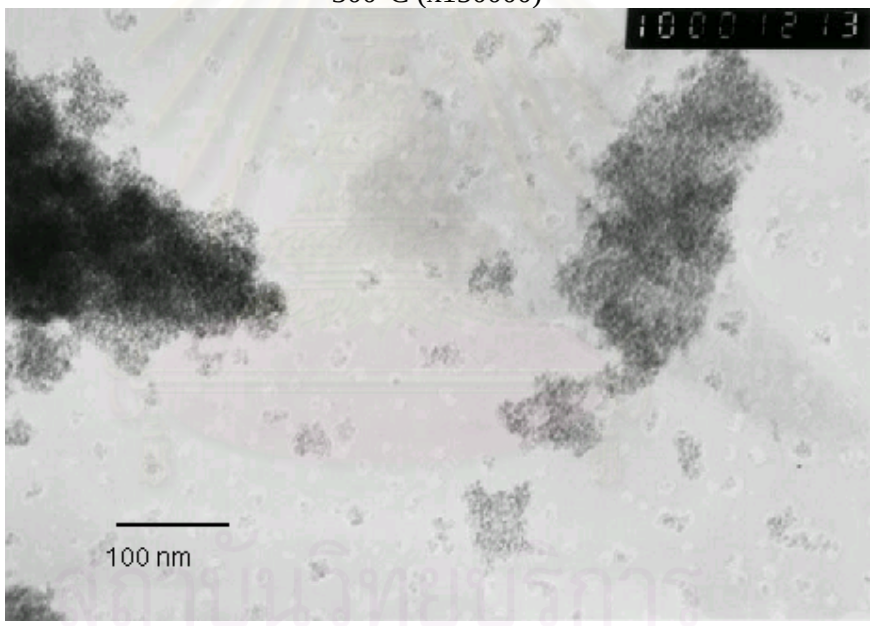

Figure 5.8 (b) TEM photograph of calcined nickel aluminate spinel at 500°C (x150000)

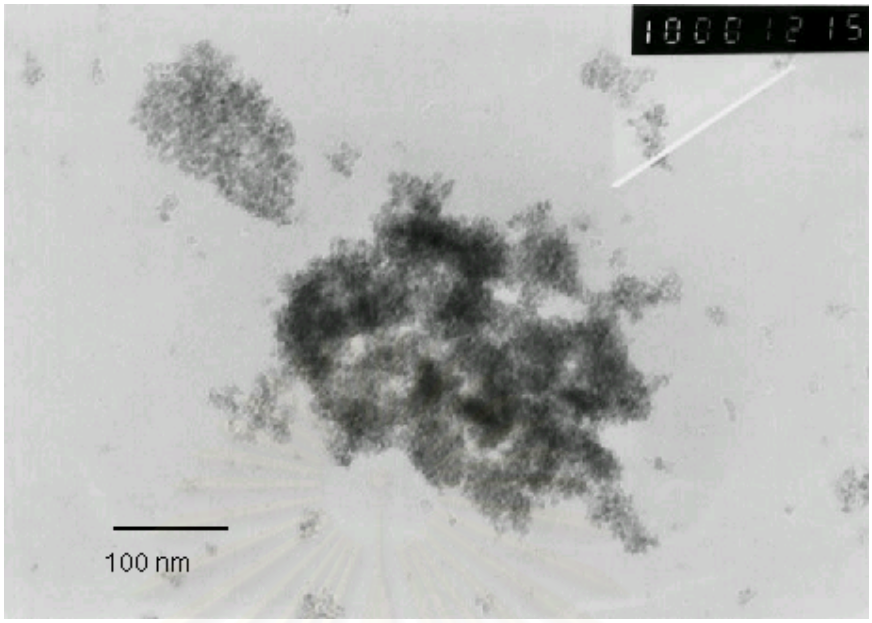

Figure 5.8 (c) TEM photograph of calcined nickel aluminate spinel at 600°C (X150000)

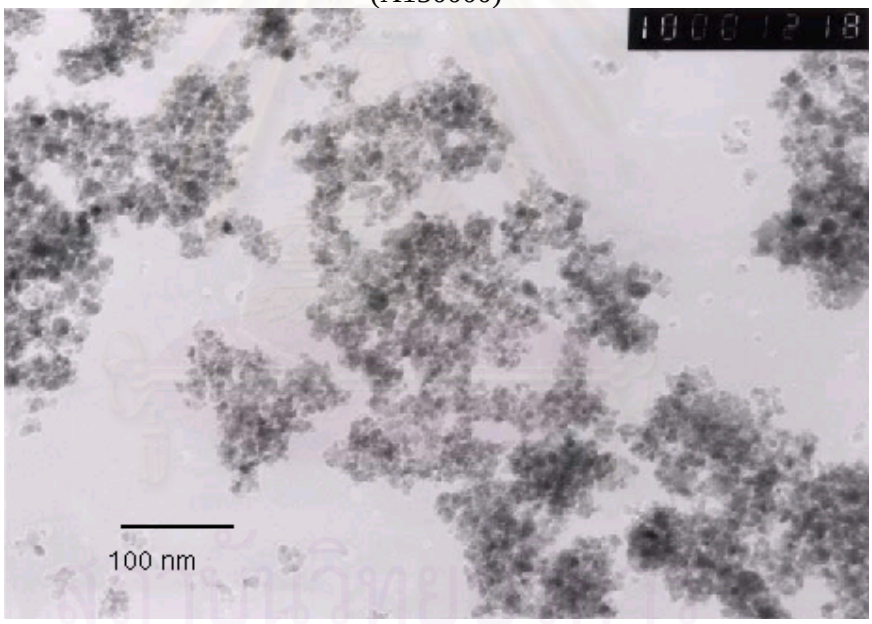

Figure 5.8 (d) TEM photograph of calcined nickel aluminate spinel at 800°C (X150000)

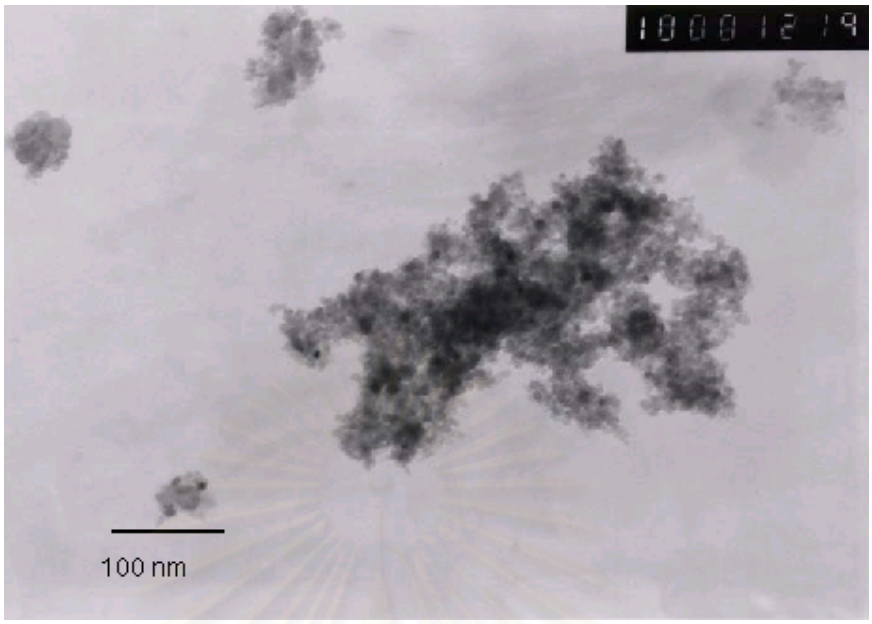

Figure 5.8 (e) TEM photograph of calcined nickel aluminate spinel at 900°C (X150000)

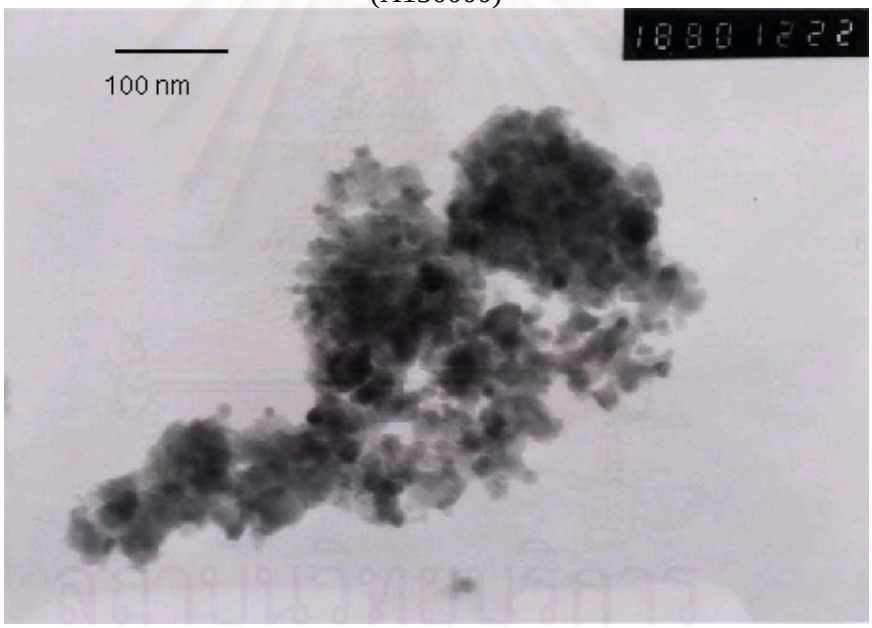

Figure 5.8 (f) TEM photograph of calcined nickel aluminate spinel at 1000°C (X150000)

5.4 Effect of the formation of spinel on the physical properties and the thermal stability of all products.

In previous section, the spinel products prepared by thermal decomposition reaction using toluene as a solvent at various reaction temperatures were described. It indicated that their properties and thermal stability could be controlled by the formation of spinel crystals at various reaction temperatures besides reaction condition and structure of starting material. Therefore, the explanation was required to clarify the occurred phenomena.

For the synthesis of cobalt aluminate, the thermal decomposition reaction of cobalt acetylacetonate and aluminum isopropoxide in toluene at various reaction

temperatures (300, 320 and 340°C) yielded nanocrystallite products having the crystallite sizes as 6.5, 6.93 and 7.02 nm. At the reaction temperature of 290°C, the obtained product had contamination of cobalt oxide. It indicated that the reaction of $CoAl_2O_4$ formation was proposed as solid-state reaction. Under inert toluene solvent conditions, thermal decomposition reaction of cobalt (II) acetylacetonate and aluminum isopropoxide were decomposed yielding $Co\text{-}O^-$ and $Al\text{-}O^-$ anions. The nucleophilic attacks of cobate ion on aluminate ion. Finally, the spinel cobalt aluminate was formed, and the amount of cobalt and aluminum in the structure depended on the amount of cobalt acetylacetonate and aluminum isopropoxide using as the starting materials. The thermal decomposition mechanism of cobalt acetylacetonate and aluminum isopropoxide in toluene can be proposed as follow [49]:

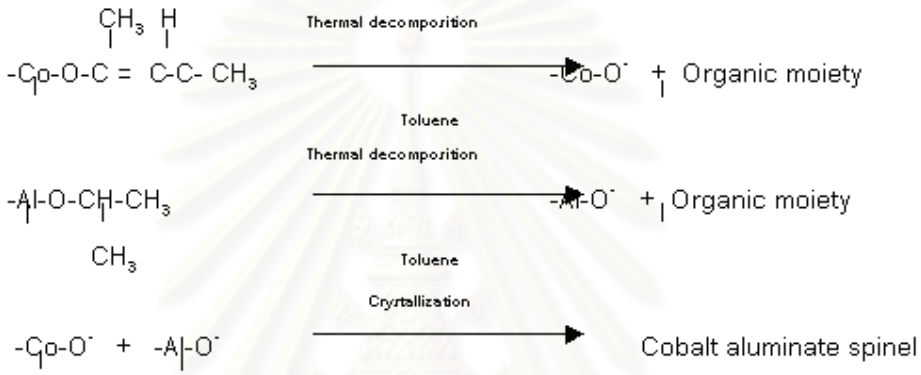

Zinc acetylacetonate and aluminum isopropoxide were formed as $Zn_xAl_yO_z$ compound at reaction temperature of 260°C. It should be indicated that the reaction of $ZnAl_2O_4$ formation was proposed as solution reaction. For the synthesis of zinc aluminate, the mechanism of zinc acetylacetonate and aluminum isopropoxide in toluene could be proposed as follow:

For the synthesis of $NiAl_2O_4$, the spinel product was formed with contaminate of nickel oxide at the reaction temperature of 290°C. It was indicated that the reaction of $NiAl_2O_4$ formation was proposed as solid-state reaction. The mechanism of nickel acetylacetonate and aluminum isopropoxide in toluene could be proposed as follow [49]:

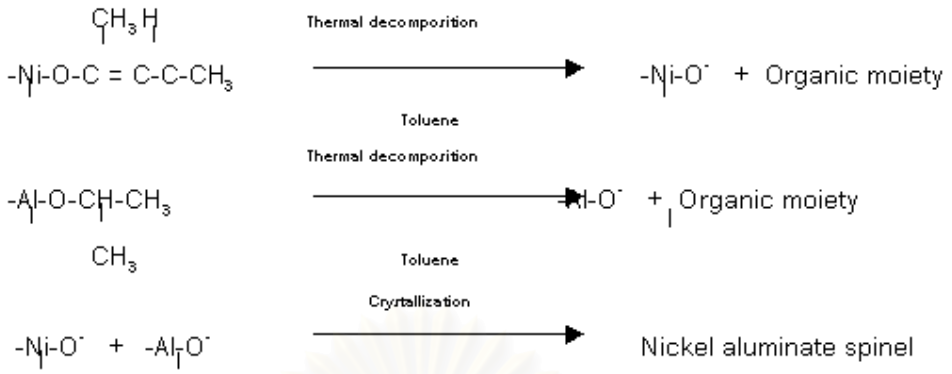

The XRD patterns of metal aluminate spinels were indicated the mechanism in the spinel formation, which were shown in Figures 5.9 to 5.11.

The formation of $CoAl_2O_4$ and $NiAl_2O_4$ spinels was independently occurred via the nucleophilic attacks of metal oxide anion and aluminum oxide anion. This might be due to the lower heat of formation of metal oxides (Co-O and Ni-O) as shown Table 5.4. The lower heat of formation of metal oxides affected the easier formation of metal oxides in the mechanism of the formation of $CoAl_2O_4$ and $NiAl_2O_4$ spinels. For the formation of $ZnAl_2O_4$ spinel, it did not occur via the nucleophilic attacks of metal oxide anion and aluminum oxide anion. This might be due to the higher heat of formation of Zn-O. The mechanism of the formation of $ZnAl_2O_4$ spinel did not occur solid-state reaction.

Table 5.4 The heat of formation of metal oxides [50]

Metal Oxide	Heat of formation, ΔH_f (kJ/mol)
Co-O	-238
Ni-O	-240
Zn-O	-350

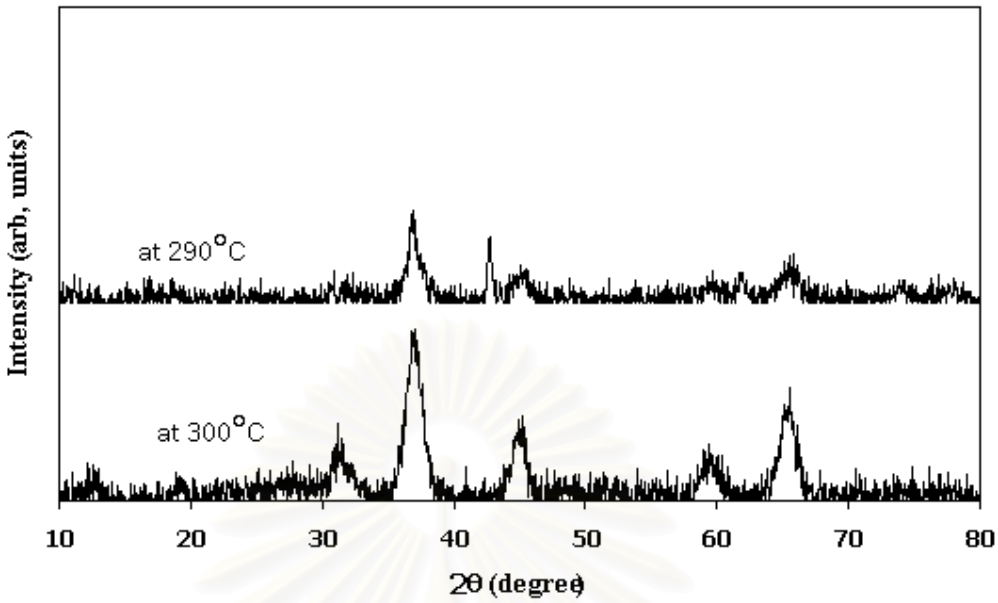

Figure 5.9 The XRD patterns of the products obtained by the reaction between cobalt acetylacetonate and aluminum isopropoxide at various reaction temperatures of 290 and 300°C

(a) The product at the reaction temperature of 290°C occurring the contamination of cobalt oxides

(b) The $CoAl_2O_4$ spinel product at the reaction temperature of 300°C disappearing the contamination of cobalt oxides and aluminum oxides

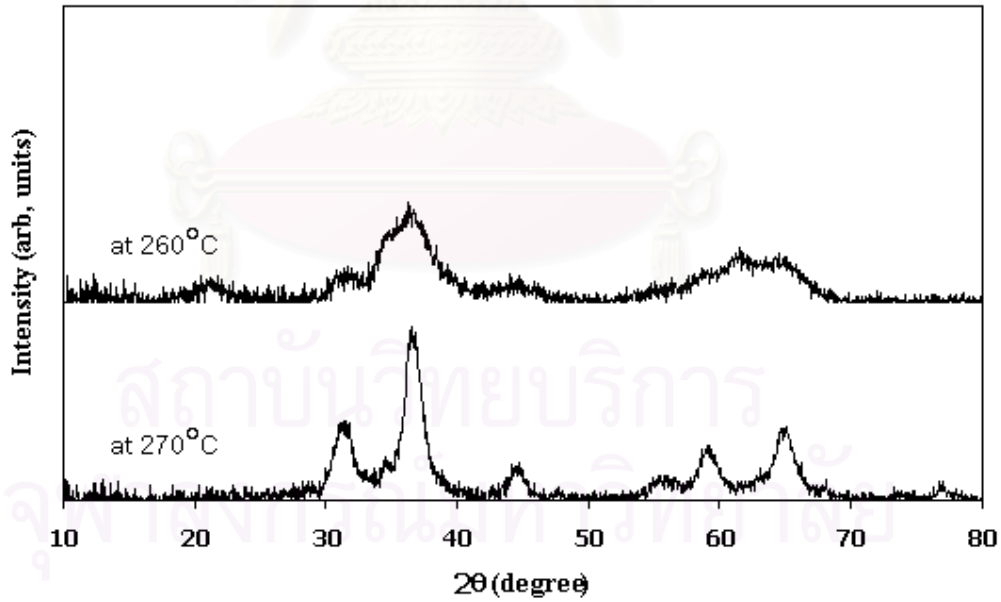

Figure 5.10 The XRD patterns of the products obtained by the reaction between zinc acetylacetonate and aluminum isopropoxide at various reaction temperatures of 260 and 270°C

(a) The product at the reaction temperature of 290°C occurring the $Zn_xAl_yO_z$ compound

(b) The $ZnAl_2O_4$ spinel product at the reaction temperature of 300°C disappearing the contamination of zinc oxides and aluminum oxides

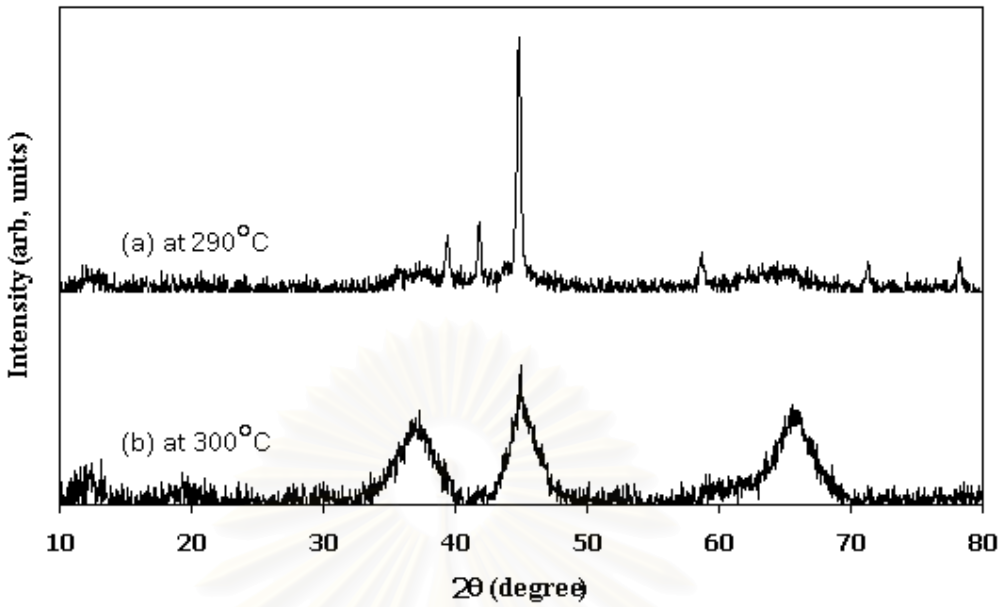

Figure 5.11 The XRD patterns of the products obtained by the reaction between nickel acetylacetonate and aluminum isopropoxide at various reaction temperatures of 290 and 300°C
(a) The product at the reaction temperature of 290°C occurring the contamination of nickel oxides
(b) The $NiAl_2O_4$ spinel product at the reaction temperature of 300°C disappearing the contamination of nickel oxides and aluminum oxides

The BET surface area data of the as-synthesized products at 300 °C for 2h before and after calcined at various temperatures of 500, 600, 800, 900 and 1000°C were determined the relation between thermal stability and the BET surface area.

In this work, thermal stability was defined as:

$$\text{Thermal stability} = \frac{\text{BET surface area at any calcination at any temperature (BET)}}{\text{BET surface area of as-synthesized sample } (BET_0)}$$

The data of the as-synthesized products at 300°C and calcined samples at various calcination temperatures, which were summarized in Tables 5.1 to 5.3, were plotted as the relation between log BET/BET_0 and $T/\sqrt{d_0}$; as synthesized product, as shown in Figure 5.12. From the curves in this figure, they were shown that the thermal stability of each spinel product was decreased with the increase of the calcination temperature because the BET surface area of each spinel products was decreased. Then, the calcination temperature had effect on the thermal stability of each spinel product. The increase of the heat-treatment temperature generates grain growth by solid-state reaction, where the driving force is the decrease of total surface energies, which comes about by grain growth [2].

In Figure 5.13, the thermal stability was performed in Table 5.5 and Table 5.6 that was defined in term of crystallize size as:

$$\text{Thermal stability} = \frac{\text{Crystallite size of calcined product at any temperature (d)}}{\text{Crystallite size of as-synthesized product } (d_0)}$$

where the thermal stability will be high if the value of d/d_0 approach to 1

From the curves in this figure, they could be determined that cobalt aluminate has higher thermal stability than zinc aluminate while thermal stability of nickel aluminate are higher than that of cobalt aluminate at the same calcination temperature of 1000°C, which were observed at the same crystallite size of the as-synthesize products; d_0.

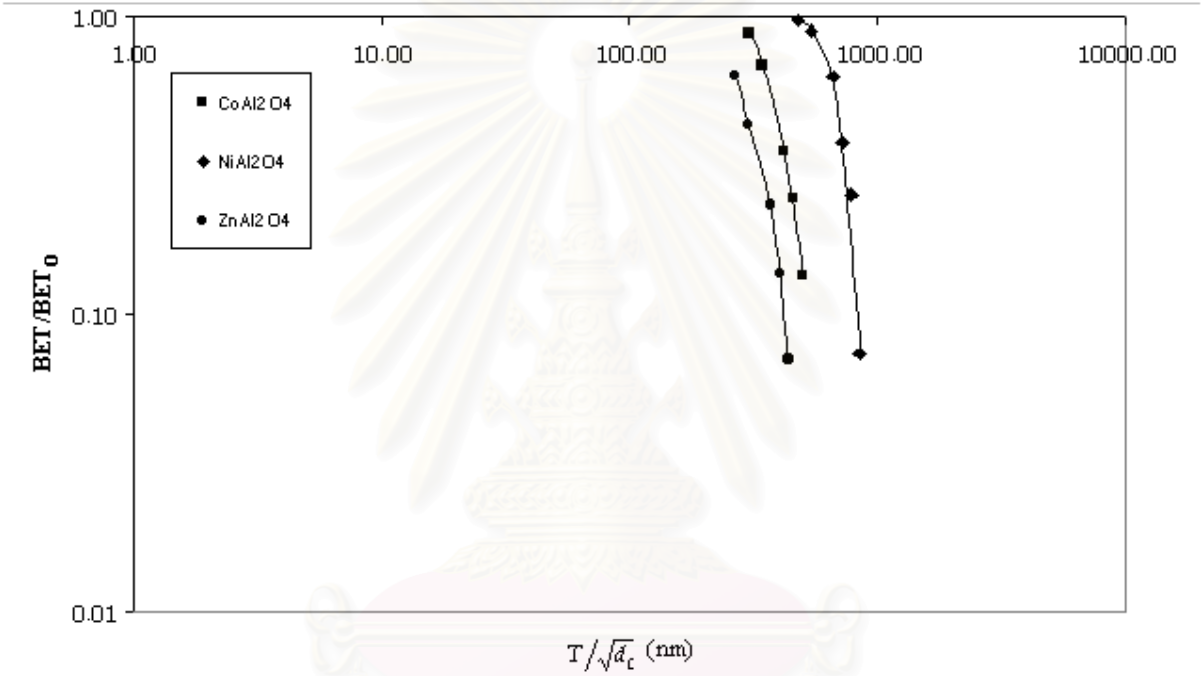

Figure 5.12 The relation between log BET/BET0 and $T/\sqrt{d_0}$ of cobalt aluminate, zinc aluminate, and nickel aluminate spinels at the reaction temperature of 300°C

Table 5.5 Nanocrystallite size of the as-synthesized spinel products at various reaction temperatures before and after calcined at 1000°C

Sample	As-synthesized Temperature	Crystallize Size (nm)		d/d_0
	T (°C)	d_0[a]	d[b]	
$CoAl_2O_4$	300	6.50	22.00	3.38
	320	6.93	21.00	3.03
	340	7.29	20.05	2.81
$ZnAl_2O_4$	270	7.62	39.28	5.15
	280	7.73	34.73	4.49
	290	8.05	33.28	4.13
	300	8.33	33.10	3.97
	320	8.61	32.79	3.81
$NiAl_2O_4$	300	2.61	13.51	5.18

[a]Crystallite size of as-synthesized product calculated from Scherrer equation using α-Al_2O_3 as an internal standard

[b]Crystallite size of calcined product at 1000°C calculated from Scherrer equation using α-Al_2O_3 as an internal standard

Table 5.6 Nanocrystallite size of the calcined spinel products at various calcination temperatures before and after calcined at 1000°C

Sample	Crystallize Size (nm)		d/d_0
	d_0[a]	d[b]	
$CoAl_2O_4$	7.46	20.42	2.74
	8.55	20.63	2.41
	13.22	22.53	1.70
$ZnAl_2O_4$	11.43	33.17	2.90
	15.52	37.63	2.42
$NiAl_2O_4$	3.65	14.23	3.90
	3.76	14.39	3.83
	4.16	14.47	3.48
	6.09	14.88	2.44
	9.16	16.13	1.76

	13.51	17.01	1.26

[a]Crystallite size of the calcined product at various temperature calculated from Scherrer equation using α-Al_2O_3 as an internal standard

[b]Crystallite size of calcined product at 1000°C calculated from Scherrer equation using α-Al_2O_3 as an internal standard

Table 5.7 The bond dissociation energy of metal oxides [51]

Metal Oxide	Bond dissociation energy (kJ/mol)
Co-O	384.5 ± 13.4
Ni-O	382.0 ± 16.7
Zn-O	159.0 ± 4.0

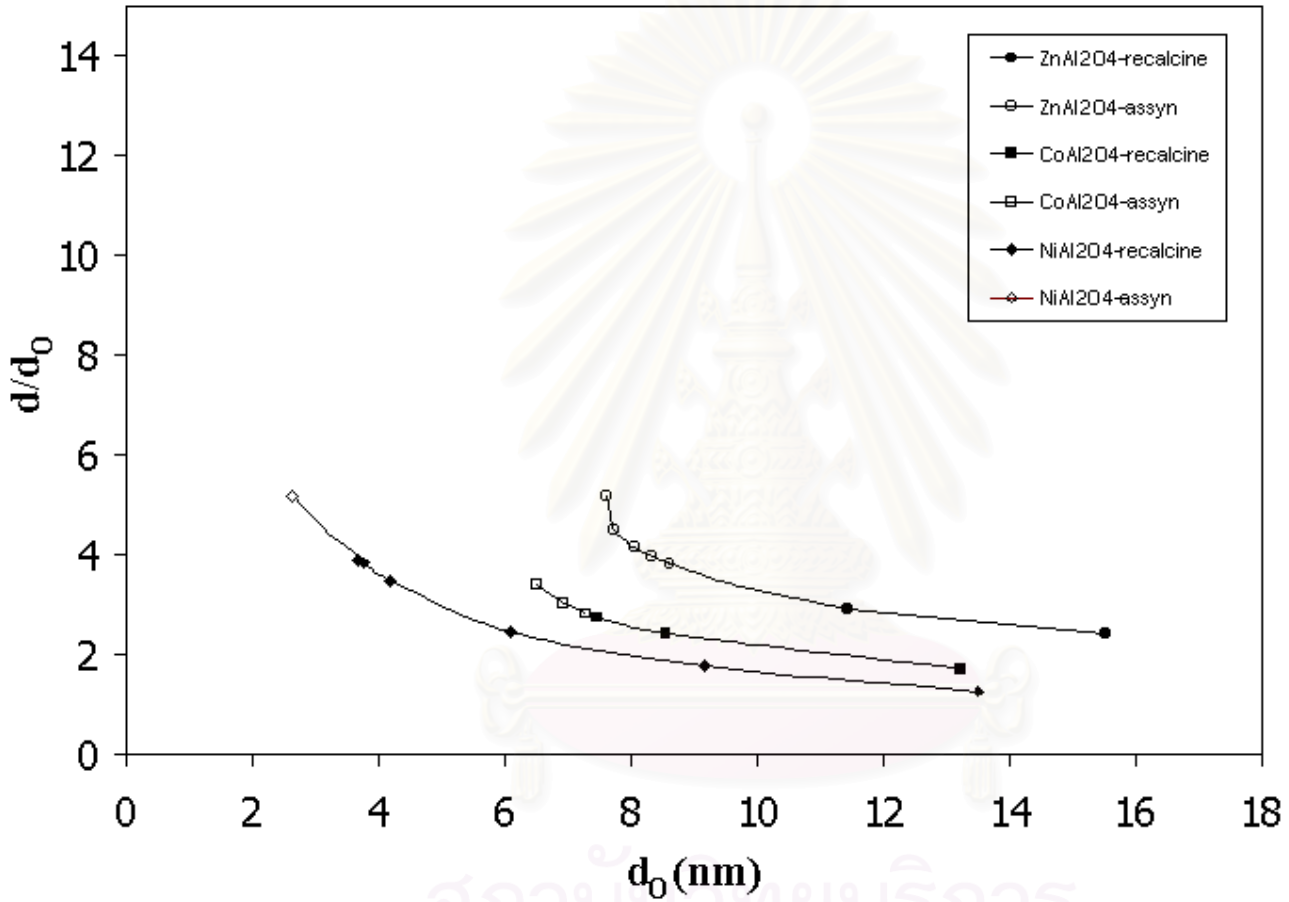

Figure 5.13 The relation between d/d_0 and d_0 of cobalt aluminate, zinc aluminate, and nickel aluminate spinels at the calcination temperature of 1000°C

However, the thermal stability of each metal aluminate spinel depended on the crystallite size of the products. The large crystals were more stable than the small crystals at the same calcination temperature. The increase of the reaction temperature of the synthesis of each spinel had effect on the increasing of crystallite size of as-synthesized product that affected the thermal stability. The large crystals had higher thermal stability than the small crystals. $CoAl_2O_4$, $ZnAl_2O_4$ and $NiAl_2O_4$ had the same trend of results. The type of metal (Co, Zn and Ni) in tetrahedral sites of metal aluminate spinels had influence on the thermal stability by the comparison between $CoAl_2O_4$, $ZnAl_2O_4$ and $NiAl_2O_4$. It is the result of the bond dissociation energy of various metal oxides (M-O) in tetrahedral sites of the spinel-type structure. The bond dissociation energy of metal oxides was performed in Table 5.7. Zn-O has the bond dissociation energy equal to 159.0 ± 4.0 kJ/mol [51], which is lower than Co-O (384.5 ± 13.4 kJ/mol) [51] and Ni-O (382.0±16.7 kJ/mol) [51]. It is observed that the lower the bond dissociation energy, the higher the thermal stability.

The bond dissociation energy of Ni-O is close to the bond dissociation energy of Co-O. The difference in the thermal stability of both spinels was explained by the different cation distribution over sites with tetrahedral coordination of the spinel-type structure. J. Bäckerman and K. D. Becker [52] mentioned that in crystals possessing a noticeable temperature dependence of the cation distribution, the kinetics of cation exchange could be studied by mean of temperature-jump relaxation experimentals. It was observed that the metal in tetrahedral sites of both cobalt aluminate and nickel aluminate is in VIIIB group of the Periodic Table. However, zinc aluminate, which has the metal (Zn) in tetrahedral site coordination, is in IIB group of the Periodic Table. The former results could be explained that the type of metal in tetrahedral sites affected the thermal stability. The metal of VIIIB group in tetrahedral sites of the spinel-type structure affected thermal stability of nickel aluminate and cobalt aluminate higher than the thermal stability of zinc aluminate that has the metal of IIB group. Then, the thermal stability of metal aluminate spinel is in the order of, $NiAl_2O_4$ > $CoAl_2O_4$ > $ZnAl_2O_4$. It means that metal of VIIIB group in tetrahedral sites had more effect than metal of IIB group on the increase of the thermal stability because of the bond dissociation energy. For the same VIIIB group, the thermal stability might depend on the cation distribution over sites with tetrahedral coordination in the spinel-type structure.

6.1 Conclusions

The conclusions of the present research are the following:

The type of divalent metal (Co, Zn and Ni) in tetrahedral sites of metal aluminate spinels affected the thermal stability that revealed in the order of:

$$NiAl_2O_4 > CoAl_2O_4 > ZnAl_2O_4$$

It is resulted from the difference of the bond dissociation energy and the cation distribution in tetrahedral sites of metal aluminate spinels.

6.2 Recommendation for the future studies

From the previous conclusions, the following recommendations for the future studies are proposed.

1. To study the effect of the other divalent transition metals of the second series in the Periodic Table on the thermal stability of metal aluminate spinels.

2. To study the thermal stability of the other spinels besides metal aluminate spinels that has Co, Zn and Ni in tetrahedral sites.

3. To verify the difference of the bond dissociation energy and the cation distribution in tetrahedral sites of spinel-type structure affected the thermal stability.

REFERENCES

1. A. Edelstein, R. C. Cammarata. Synthesis, Properties and Applications, Nanomaterials. Institute of physics Publishing, Bristol and Philadelphia, 1996.
2. W. S. Cho, and M. Kakihana. Crystallization of ceramic pigment $CoAl_2O_4$ nanocrystals from Co-Al metal organic precursor. J. Alloy. Compd. 287 (1999): 87-90.
3. T. Mimani. Instant synthesis of nanoscale spinel aluminates. J. Alloy. Compd. 315 (2001): 123-128.
4. M. Zayat, and D. Levy. Blue $CoAl_2O_4$ particles prepared by the sol-gel and citrate-gel methods. Chem. Mater. 12 (2000): 2763-2769.
5. G. E. Bacon, and F. F. Roberts. Neutron-diffraction studies of magnesium ferrite-aluminate powders. Acta Cryst. 6 (1953): 57-62.
6. S. Chokkaram, R. Srinivasan, and D. R. Milburn. Conversion of 2-octanol over nickel-alumina, cobalt-alumina, and alumina catalysts. J. Mol. Catal. A-Chem. 121 (1997): 157-169.
7. C. O. Arean, M. P. Mentruit, E. E. Platero, F. X. L. I. Xamena, and J. B. Parra. Sol-gel method for preparing high surface area CoAl2O4 and Al2O3-CoAl2O4 spinels. Mater. Lett. 39 (1999): 22-27
8. J.A. Toledo, M.A. Valenzuela, and H. Armendariz, "Oxidative dehydrogenation of 1-butene to butadiene on alpha-$Fe_2O_3/ZnAl_2O_4$ and $ZnFe_XAl_2$-xO_4 catalysts", Catal. Lett. 30 (1995): 279-288.
9. A. A. Khassin, T. M. Yurieva, G. N. Kustova, I. S. Itenberg, M. P. Demeshkina, T. A. Krieger, and L. M. Plyasova. Cobalt-aluminum co-precipitated catalysts and their performance in the Fischer-Tropsch synthesis. J. Mol. Cat. A-Chem. 168 (2001): 193-207.
10. S. Chamlal, A. Larbot, M. Persin, J. Sarrazin, M. Sghyar, and M. Rafiq. Cobalt spinel $CoAl_2O_4$ via sol-gel process: elaboration and surface properties. Mater. Res. Bull. 35 (2000): 2515-2523.
11. M. A. Valenzuela, J. P. Jacobs, and P. Bosch. The influence of the preparation method on the surface structure of $ZnAl_2O_4$. Appl. Catal. A 148 (1997): 315-324.
12. M. Zawadzki, and J. Wrzyszcz. Hydrothermal synthesis og nanoporous zinc aluminate with high surface area, Mater. Res. Bull. 35 (2000): 109-114.
13. M. Zawadzki, W. MistaMi□ta, and L. KepinskiKepi□ski. Metal-support effects of platinum supported on zinc aluminate. Vacuum 63 (2001): 291-296.
14. M. A. Valenzuela, P. Bosch, and G. AguilarRios. Comparison between sol-gel, coprecipitation and mixing synthesis of $ZnAl_2O_4$. J. Sol-Gel Sci. Techn. 8 (1997): 107-110.

15. G. Nolven P. Michel, Catalytic Combustion of Methane: Copper Oxide supported on High-Specific-area Spinels synthesized by a Sol-Gel Process, J. Chem. Soc. Faraday. Trans. 90 (1994): 1541-1546.
16. J. Wrzyszcz, M. Zawadzki, J. Trawczy□ski, H. Grabowska, and W. Mi□ta. Some catalytic properties of hydrothermally synthesized zinc aluminate spinel. Appl. Catal. A 210 (2001): 263-269.
17. Y. Cesteros, P. Salagre, F. Medina, and J. E. Sueiras. Synthesis and characterization of several $Ni/NiAl_2O_4$ catalysts active for the 1,2,4-trichlorobenzene hydrodechlorination. Appl. Catal. B 25 (2000): 213-227.
18. J. A. Pena, J. Herguido, C. Guimon, A. Monzon, and J. Santamaria. Hydrogenation of acetylene over Ni/NiAl2O4 catalyst: Characterization, coking, and reaction studies. J. Catal. 159 (1996): 313-322.
19. O. Arean, M. P. Mentruit, A. J. L. Lopez, and J. B. Parra. High surface area nickel aluminate spinels prepared by a sol-gel method. Coll. and Surf. A-Physicochem & Eng Aspects 180 (2001): 253-258.
20. F. Meyer, A. Dierstein, Ch. Beck, W. Härtl, R. Hempelmann, S. Mathur, and M. Veith. Size-controlled synthesis of nanoscaled aluminum spinels using heterobimetallic alkoxide precursors via water/oil microemulsions. Nanostructured Mater. 12 (1999): 71-74.
21. M. Inoue, H. Otsu, Synthesis of submicron sperical crystals of gadolinium gallium garmets by the glycothermal method, J. Mater. Sci. Lett. 14 (1995): 1303-1305.
22. M. Inoue, H. Tanino, Formation of microcrystalline -alumina by glycothermal treatment of gibbsite, J. Am. Cerm. Soc. 72 (1998): 352-353.
23. M. Inoue, H. Kominami, Thermal transformation of □ -alumina formed by thermal decomposition of aluminum alkoxide in organic media, J. Am. Ceram. Soc. 75 (1992): 2597-2598.
24. M. Inoue, and H. Kominami, Novel synthesis method for the catalytic use of thermally stable zirconia: Thermal decomposition of zirconia alkoxide in organic media. Appl. Catal. A 97 (1993): L25-L30.
25. T. Ohgushi, and S. Umeno. Low temperature synthesis of dispersed fine particle of cobalt aluminate-a new application of zeolite. Bull. Chem. Soc. Jap. 60 (1987): 4457-4458.
26. A. J. Faneli, and J.V. Burlew. Preparation of alumina powder in alcohol. J. Mater. Sci. 23(1998): 2897-2904.
27. Y. Oguri, and R. E. Riman. Processing of anatase prepared from hydrothermally treated alkoxy-derived hydrous titania. J. Mater. Sci. 23 (1988): 2897-2904.
28. M. Kondo, and K. Shinozaki. Crystallization behavior and microstructure of hydrothermal treated monodispersed titanium dioxide particles. J. Ceram. Soc. Jap. 102 (1994): 740-744.
29. M. Inoue, and Y. Kondo. An ethylene glycol derivative of boehmite. Inorg. Chem. 27 (1998): 215-221.
30. M. Inoue, and H. Kominami. Novel synthesis method for thermally stable monoclinic zirconia: Hydrolysis of zirconia alkoxides at high temperature with a limited amount of water dissolved in inert organic solvent form the gas phase. Appl. Catal. A 121 (1995): L1-L5.
31. M. Inoue, and H. Otsu. Glycothermal synthesis of rare earth aluminium garnets. J. Alloy Compd. 226 (1995): 146-151.
32. T. Ohtake, N. Sonoyama, and T. Sakata. Elecreochemical luminescence of $ZnGa_2O_4$ and $ZnGa_2O_4$: Mn electrodes. Chem. Phys. Lett. 298 (1998): 395-399.

33. M. Inoue, and T. Nishikawa. Reaction of rare earth acetates with aluminum isopropoxide in ethylene glycol: Synthesis of the garnet and monoclinic phases of rare earth aluminate. J. Mater. Sci. 33 (1998): 5895-5841.
34. M. Inoue, and T. Inui. Glycothermal synthesis of metastable phases, 9th Cimtec-World Ceramics Congress, Ceramics: Getting into the 2000's-Part B: 41-48.
35. M. Inoue, H. Kominami, H. Otsu, and T. Inui. Synthesis of mycrocrystalline titania in organic media. Nippon Kagaku Kaishi (1991): 1364.
36. H. Kominami, J. Kato, Y. Doushi, B. Ohtani, S. Nishimoto, M. Inoue, T. Inui and Y. Kera. Novel synthesis ofmicrocrystalline titanium (IV) oxide having high thermal stability and ultra-high photocatalytic activity: Thermal decomposition of titanium (IV) alkoxide in organic solvents. Catal. Lett. 46 (1997): 235-240.
37. H. Kominami, Y. Takada, H. Yamagiwa and Y. Kera, Synthesis of thermal stable nanocrystalline anatase bt high-temperature hydrolysis of titanium alkoxide with water water dissolved in orgainc solvent from gas phase, J. Mater. Sci. Lett. 15 (1996): 197-199.
38. H. Kominami, M. Kohno, Y. Takada, M. Inoue, T. Inui and Y. Kera, Hydrolysis of titanium alkoxide in organic solvent at high temperatures: A new synthetic method for nanosized, thermal stable titanium (IV) oxide, Ind. Eng. Chem. Res. 38 (1999): 3925-3931.
39. M. Inoue and T. Inui, Glycothermal synthesis of metastable phases, 9th Cimtec-World Ceramics Congress, Ceramics: Getting into the 2,000's-Part B: 41-48.
40. B. M. Reddy, S. Mehdi and E. P. Reddy, Synthesis of alkoxyalumoxanes by oxidation of aluminum metal in alcohols, 9th Cimtec-World Ceramics Congress, Ceramics: Getting into the 2,000's-Part D: 593-598.
41. K. Othmer. Encyclopedia of Chemical technology. 4th edition, A wiley-Interscience Publication, John Wiley & Sons, 2 (1991): 184-220.
42. K. Othmer. Encyclopedia of Chemical technology. 4th edition, A wiley-Interscience Publication, John Wiley & Sons, 6 (1991): 760-892.
43. K. Othmer. Encyclopedia of Chemical technology. 4th edition, A wiley-Interscience Publication, John Wiley & Sons, 17 (1991): 1-42.
44. K. Othmer. Encyclopedia of Chemical technology. 4th edition, A wiley-Interscience Publication, John Wiley & Sons, 25 (1998): 789-853.
45. K. Othmer. Encyclopedia of Chemical technology. 3th edition, A wiley-Interscience Publication, John Wiley & Sons, (1978).
46. A. R. West. Basic solid state chemistry. 2th edition, London, John Wiley & Sons, (1999).
47. D. K. Chakrabarty. Solid state chemistry. New Age International Limited, Publishers, New Delhi. (1996).

48. A. R. West. Solid state chemistry and its applications. London, John Wiley & Sons, (1997).

49. P. Sangthonganothai. Solvothermal synthesis of spinel-type zinc gallate and zinc aluminate powders. Master's thesis, Faculty of Engineering, Chulalongkorn University, (2000).

50. G. H. Aylward. SI Chemical Data. 5th edition, John Wiley & Sons, Australia, (2002).

51. D. R. Lide. CRC Handbook of Chemistry and Physics. CRC Press, New York, 81st edition, (2000-2001).

52. J. Bäckermann, and K. D. Becker. The mechanism of cation equilibration in nickel aluminate spinel, $NiAl_2O_4$. Z. Phys. Chem. 206 (1998): 31-47.

APPENDICES

APPENDIX A

CALCULATION OF THE AMOUNT OF THE REACTANT USED

In this study, cobalt aluminate, zinc aluminate, and nickel aluminate, which were the spinel-type structures, were prepared using toluene as a solvent with the molar ratio of 0.5.

A.1 Calculation of cobalt aluminate preparation

Cobalt (II) acetylacetonate and aluminum isopropoxide are used as the reactants for the preparing of cobalt aluminate powder.

1. Cobalt (II) acetylacetonate $[CH_3COCH=C(O-)CH_3]_2Co$ has molecular weight of 257.15 g/mol.

   Cobalt, Co, has atomic weight of 58.933 g/mol.

2. Aluminium Isopropoxide (AIP, $[(CH_3)_2CHO]_3Al$) has molecular weight of 204.25 g/mol.

   Aluminum, Al, has atomic weight of 26.9815 g/mol.

Example A.1: Calculation of preparation of cobalt aluminate with molar ratio Co/Al = 0.5 is shown as follow:

Aluminum isopropoxide 15 g were used for preparation of cobalt aluminate with molar ratio Co/Al = 0.5.

The reagent 15 g were consisted of cobalt equal to:

Aluminium = (26.9815/204.25) x 15 = 1.9815 g = 0.07344 mol

cobalt equal to:

Cobalt = 0.5 x 0.07344 mol = 0.03672 mol = 2.1640 g

From cobalt = 2.1640 g, cobalt acetylacetonate is used equal to:

So, weight of cobalt acetylacetonate = (257.15/58.933) x 2.1640 g = 9.4425 g

A.2 Calculation of zinc aluminate preparation

Zinc (II) acetylacetonate and aluminum isopropoxide are used as the reactants for the preparing of zinc aluminate powder.

1. Zinc (II) acetylacetonate $[CH_3COCH=C(O-)CH_3]_2Zn$ has molecular weight of 263.59 g/mol.

   Zinc, Zn, has atomic weight of 65.37 g/mol.

2. Aluminium Isopropoxide (AIP, $[(CH_3)_2CHO]_3Al$) has molecular weight of 204.25 g/mol.

   Aluminum, Al, has atomic weight of 26.9815 g/mol.

Example A.2: Calculation of preparation of zinc aluminate with molar ratio Zn/Al = 0.5 is shown as follow:

Aluminum isopropoxide 15 g were used for preparation of zinc aluminate with molar ratio Zn/Al = 0.5.

The reagent 15 g were consisted of Zinc equal to:

Aluminium = (26.9815/204.25) x 15 = 1.9815 g = 0.07344 mol

zinc equal to:

Zinc = 0.5 x 0.07344 mol = 0.03672 mol = 2.40039 g

From zinc = 2.40039 g, zinc acetylacetonate is used equal to:

So, weight of zinc acetylacetonate = (263.59/65.37) x 2.40039 g = 9.6790 g

A.3 Calculation of nickel aluminate preparation

Nickel (II) acetylacetonate and aluminum isopropoxide are used as the reactants for the preparing of nickel aluminate powder.

1. Nickel (II) acetylacetonate $[CH_3COCH=C(O-)CH_3]_2Ni$ has molecular weight of 256.91g/mol.

   Nickel, Ni, has atomic weight of 58.70 g/mol.

2. Aluminium Isopropoxide (AIP, $[(CH_3)_2CHO]_3Al$) has molecular weight of 204.25 g/mol.

   Aluminum, Al, has atomic weight of 26.9815 g/mol.

Example A.3: Calculation of preparation of nickel aluminate with molar ratio Ni/Al = 0.5 is shown as follow:

Aluminum isopropoxide 15 g were used for preparation of nickel aluminate with molar ratio Co/Al = 0.5. The reagent 15 g were consisted of nickel equal to:

Aluminium = (26.9815/204.25) x 15 = 1.9815 g = 0.07344 mol

nickel equal to:

Nickel = 0.5 x 0.07344 mol = 0.03672 mol = 2.1555 g

From nickel = 2.1640 g, nickel acetylacetonate is used equal to:

So, weight of nickel acetylacetonate = (256.91/58.70) x 2.1555 g = 9.4339 g

APPENDIX B

CALCULATION OF THE CRYSTALLITE SIZE

Calculation of the crystallite size by Scherrer equation

The crystallite size was calculated from the half-height width of the diffraction peak of spinel-type structures such as cobalt aluminate, zinc aluminate, and nickel aluminate using the Scherrer equation. The value of the shape factor, K was taken to be 0.9 and □-alumina was used to be internal standard.

From Scherrer equation:

$$D = \frac{K\lambda}{\beta \cos\theta} \qquad \text{(B.1)}$$

where, D = Crystallite size

K = Crystallite-shape factor = 0.9

λ = X-ray wavelength, for CuKα = 1.5418 Å

θ = Observed peak angle

β = X-ray diffraction broadening, rad

$$\beta^2 = \beta_P^2 - \beta_R^2 \qquad \text{(B.2)}$$

$$\beta = \sqrt{\beta_P^2 - \beta_R^2}$$

where, β_P = The measured peak width in radians at half peak height.

β_R = The corresponding width of a standard material.

The X-ray diffraction broadening is the pure breadth of a powder reflection free of all broadening due to the experimental equipment, by using Warren's correction for instrumental broadening. Standard α-alumina is used to observe the instrumental broadening.

Example B.1: The crystallite size of pure cobalt aluminate

The measured peak width $= 37.6987° - 36.3852°$

$= 1.3135°$

$= 2.2925 \times 10^{-2}$ rad

The corresponding width of α-alumina as an internal standard

$= 4.3700 \times 10^{-3}$ rad

The pure diffraction profile $= \sqrt{\beta_P^2 - \beta_R^2}$ rad

$= \sqrt{(2.2925 \times 10^{-2})^2 - (4.3700 \times 10^{-3})^2}$ rad

$\beta = 2.2250 \times 10^{-2}$ rad

$2\theta = 37.1200°$

$\theta = 18.56°$

$\lambda = 1.5418$ Å

The crystallite size $= \dfrac{0.9 \times 1.5418}{0.02250 \times \cos\left(\dfrac{37.12}{2}\right)}$ Å

$= 64.9917$ Å

$D = 6.50$ nm

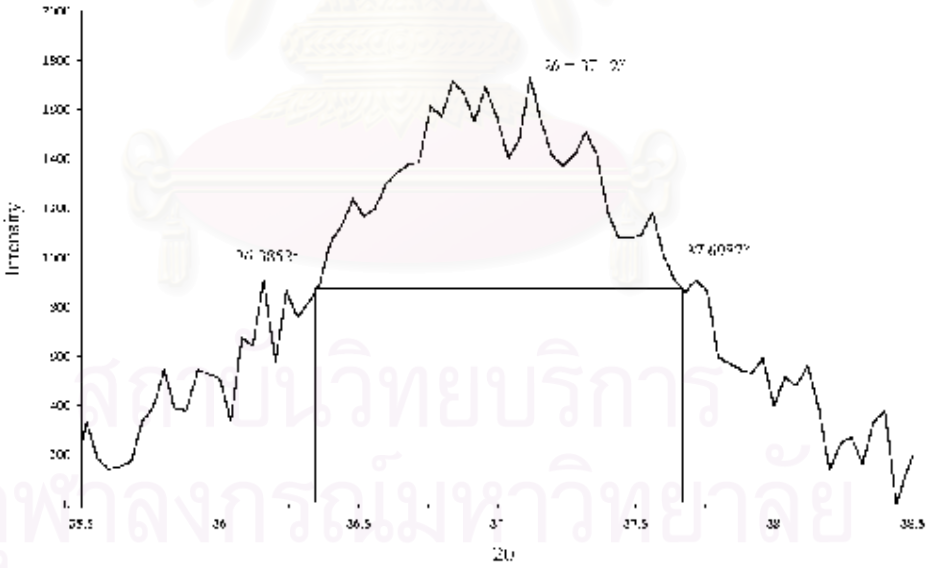

Figure B.1 The measured peak of cobalt aluminate to calculate the crystallite size.

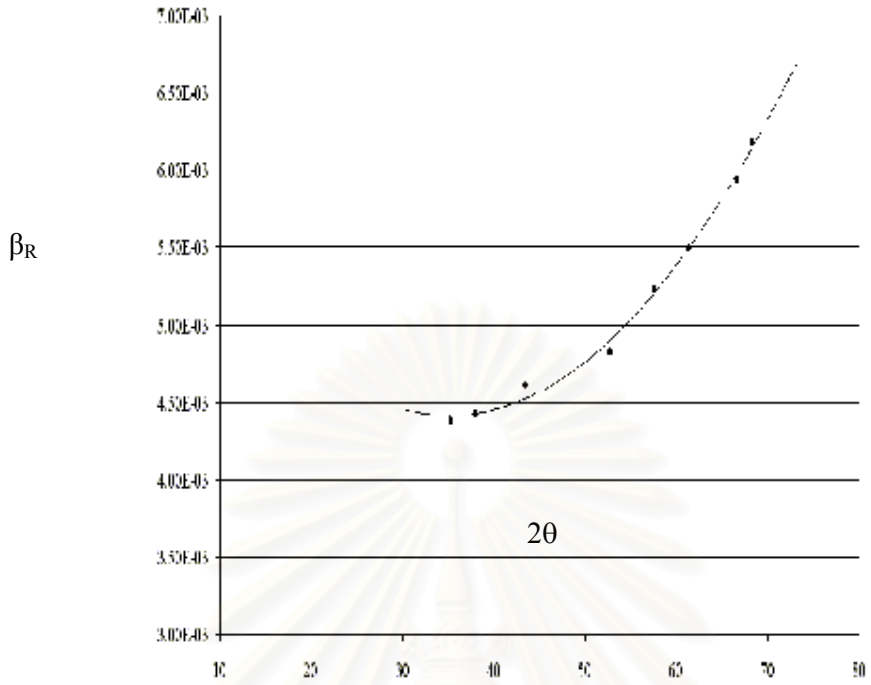

Figure B.2 The graph indicating the value of the line broadening attribute to the experimental equipment from the α-alumina standard.

APPENDIX C

CALCULATION OF THE SPECIFIC SURFACE AREA

From Brunauer-Emmett-Teller (BET) equation

$$\frac{p}{n(1-p)} = \frac{1}{n_m C} + \frac{(C-1)p}{n_m C} \qquad (C.1)$$

Where, p = Relative partial pressure of adsorbed gas, P/P_0

P_0 = Saturated vapor pressure of adsorbed gas in the condensed state at the experimental temperature, atm

P = Equilibrium vapor pressure of adsorbed gas, atm

n = Gas adsorbed at pressure P, ml. at the NTP/g of sample

n_m = Gas adsorbed at monolayer, ml. at the NTP/g of sample

C = Exp $[(H_C - H_1)/RT]$

H_C = Heat of condensation of adsorbed gas on all other layers

H_1 = Heat of adsorption into the first layer

Assume $C \longrightarrow \infty$, then

$$\frac{p}{n(1-p)} = \frac{p}{n_m}$$

$$n_m = n(1 - p) \qquad (C.2)$$

The surface area, S, of the catalyst is given by

$$S = S_b \times n_m \qquad (C.3)$$

From the gas law

$$\frac{P_b V}{T_b} = \frac{P_t V}{T_t} \qquad (C.4)$$

Where, P_b = Pressure at 0°C

P_t = Pressure at t°C

T_b = Temperature at 0°C = 273.15 K

T_t = Temperature at t°C = 273.15 + t K

V = Constant volume

Then, $P_b = (273.15/T_t) \times P_t = 1$ atm

Partial pressure

$$P = \frac{[\text{Flow of } (He + N_2) - \text{Flow of } He]}{\text{Flow of } (He + N_2)} \qquad (C.5)$$

$$= 0.3 \text{ atm}$$

For nitrogen gas, the saturated vapor pressure equals to

$P_0 = 1.1$ atm

then, $p = P/P_0 = 0.3/1.1 = 0.2727$

To measure the volume of nitrogen adsorbed, n

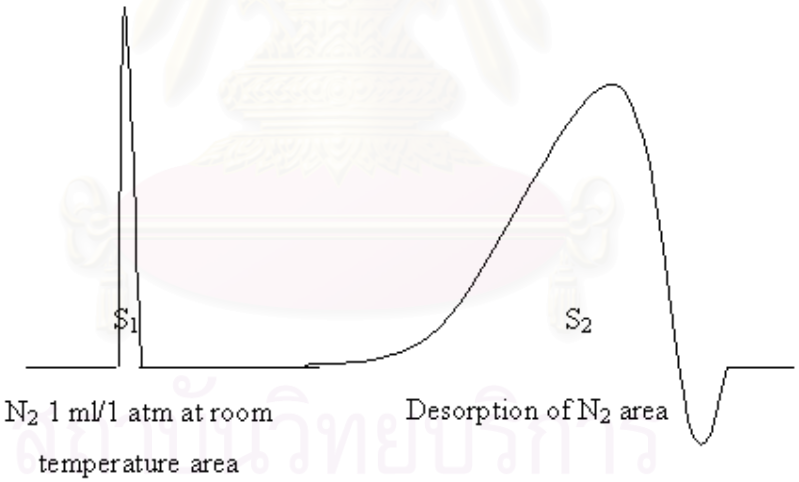

$$n = \frac{S_2}{S_1} \times \frac{1}{W} \times \frac{273.15}{T} \text{ ml. /g of catalyst} \qquad (C.6)$$

Where, S_1 = N_2 1 ml/1 atm at room temperature area

S_2 = Desorption of N_2 area

W = Sample weight, g

T = Room temperature, K

Therefore,

$$n_m = \frac{S_2}{S_1} \times \frac{1}{W} \times \frac{273.15}{T} \times (1 - p)$$

$$n_m = \frac{S_2}{S_1} \times \frac{1}{W} \times \frac{273.15}{T} \times 0.7272 \qquad (C.7)$$

Whereas, the surface area of nitrogen gas from literature equal to

S_b = 4.373 m^2/ml of nitrogen gas

Then,

$$S = \frac{S_2}{S_1} \times \frac{1}{W} \times \frac{273.15}{T} \times 0.7272 \times 4.343$$

$$S = \frac{S_2}{S_1} \times \frac{1}{W} \times \frac{273.15}{T} \times 3.1582 \text{ } m^2/g \qquad (C.8)$$

APPENDIX D

CALCULATION OF THE CRYSTALLITE SIZE

FROM TEM PHOTOGRAPH

The crystallite sizes were calculated by measurement from TEM photograph of the as-synthesized products and calcined products of the spinel-type structure as follow:

Example D.1: The measurement of the as-synthesized crystallite size of cobalt aluminate prepared using toluene as a solvent at the reaction temperature of 300°C for 2h.

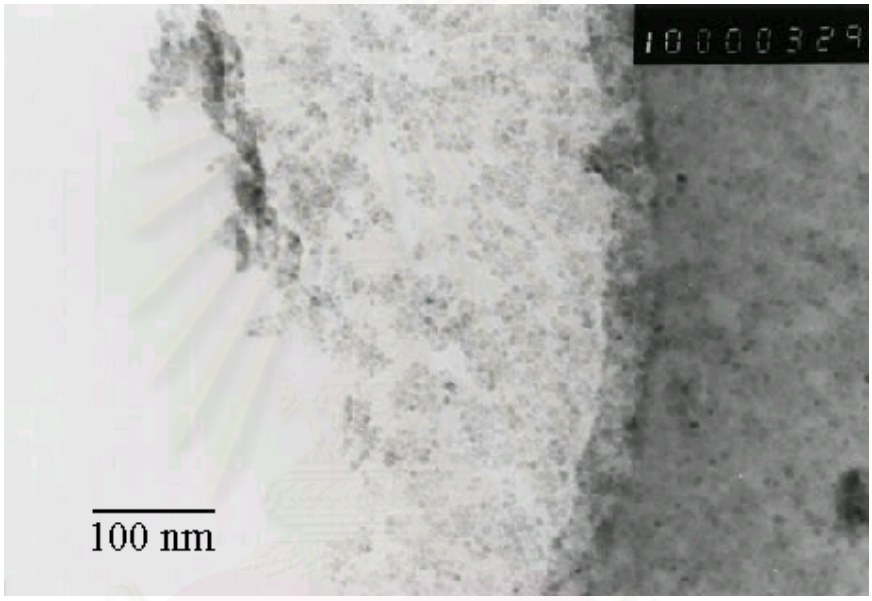

Figure D.1 TEM photograph of as-synthesized cobalt aluminate at reaction temperature of 300 °C.

At x150000 magnification, the scale is

150 mm = 1 μm

= 1000 nm

From TEM photograph, it was found that the crystallite size of the particles closed to each other and that was 0.8 mm. Therefore, the crystallite size observed by TEM is

$$\text{Crystallite size} = \frac{1000\ \text{nm}}{150\ \text{mm}} \times 0.95\ \text{mm}$$

$$\text{Crystallite size} = 6.33\ \text{nm}$$

Example D.2: The measurement of the calcined crystallite size of cobalt aluminate at the calcination temperature of 1000°C that prepared using toluene as a solvent with the reaction temperature of 300°C for 2h.

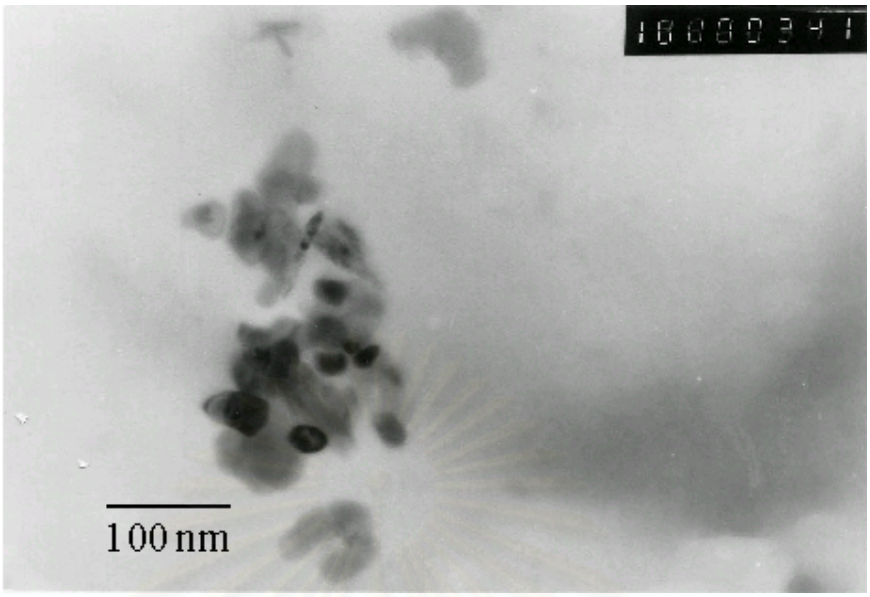

Figure D.2 TEM photograph of calcined cobalt aluminate at the calcination temperature of 1000°C that prepared with the reaction temperature of 300°C.

At x150000 magnification, the scale is

150 mm = 1 μm

= 1000 nm

From TEM photograph, it was found that the distribution of the crystallite size of the calcined product was broad. Therefore, the crystallite size observed by TEM photograph was averaged.

The measured crystallite sizes from TEM photograph were 3.4, 3.0, 3.0, 3.1, 3.2, 3.6, 3.4, 2.8, 3.8, 3.8, 3.0, 3.5 and 3.3. The average crystallite size was

$$\text{Crystallite size} = \frac{3.4+3.0+3.0+3.1+3.2+3.6+3.4+2.8+3.8+3.8+3.0+3.5+3.3}{13}$$

$$= 3.30 \text{ mm}$$

Therefore, the crystallite size measured by TEM is

$$\text{Crystallite size} = \frac{1000 \text{ nm}}{150 \text{ mm}} \times 3.30 \text{ mm}$$

$$\text{Crystallite size} = 22.00 \text{ nm}$$

APPENDIX E

CALCULATION OF THE PARTICLE SIZE DISTRIBUTION

The particle size data of $CoAl_2O_4$, $ZnAl_2O_4$ and $NiAl_2O_4$ spinels at the reaction temperatures of 300°C were calculated by measurement from TEM photograph, which were summarized in Table E.1.

Table E.1 The particle size of $CoAl_2O_4$, $ZnAl_2O_4$ and $NiAl_2O_4$ spinels at the reaction temperatures of 300°C (The number of the measured particles of each spinels equal to 50 particles)

Sample	As-synthesized Temperature (°C)	Particle Size (nm)	Number (%)
$CoAl_2O_4$	300	6.00	10
		6 . 1 3	5
		6 . 3 3	6 0
		6.40	2
		6.47	15
		6.60	8
$ZnAl_2O_4$	300	6.67	3
		7.00	4
		7.33	9
		7.67	7
		8.20	45
		8.67	32
$NiAl_2O_4$	300	1.87	6
		2.00	8
		2.07	12
		2.13	39
		2.20	17
		2.40	18

From Table E.1, the particle size data of metal aluminate spinel were plotted as the relation between the particle size (nm) and number (%) of metal aluminate particles, which were shown in Figures E.1 to E.3. They performed the particle size distribution of metal aluminate spinel products.

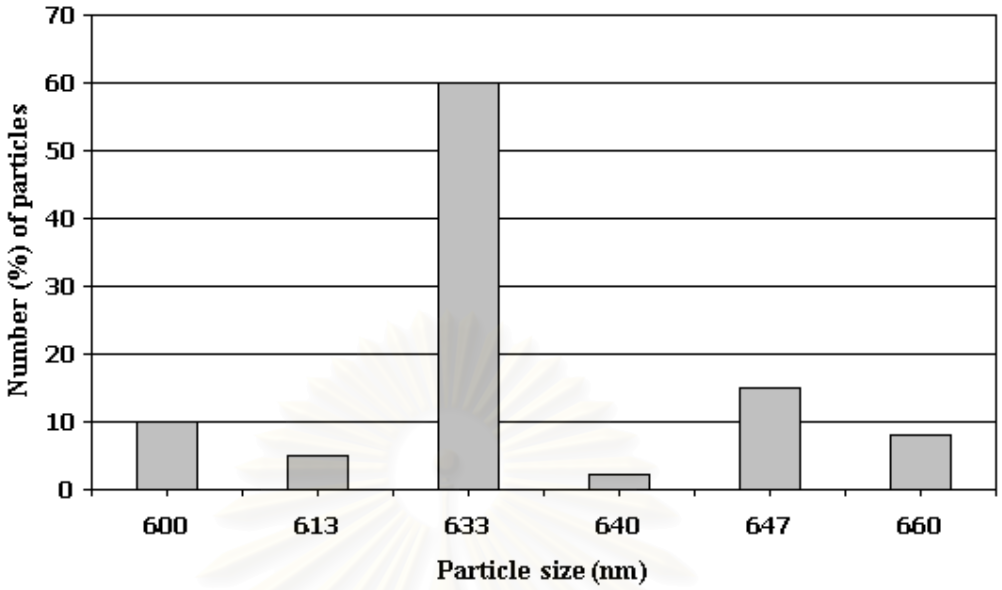

Figure E.1 The relation between the particle size (nm) and number (%) of $CoAl_2O_4$ spinel particles at reaction temperature of 300°C

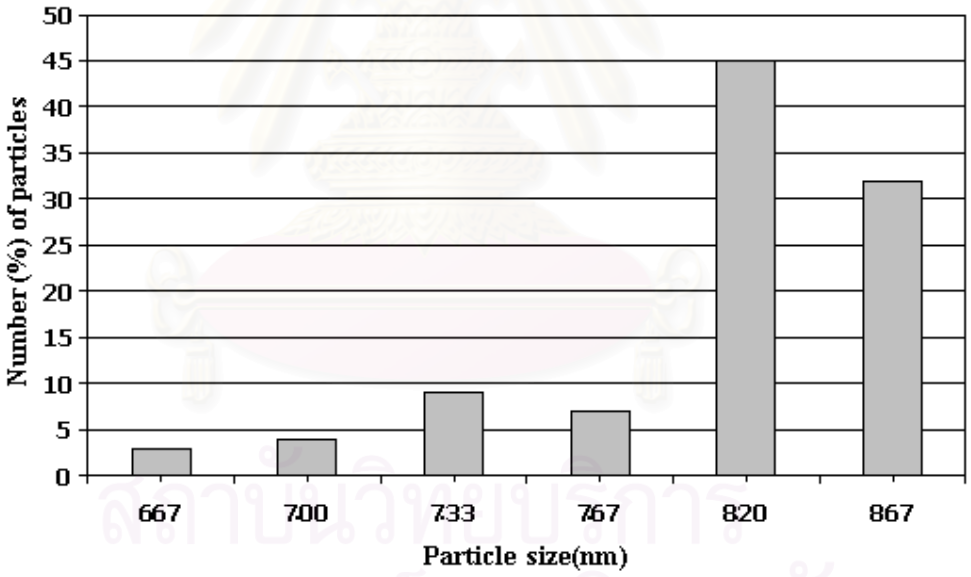

Figure E.2 The relation between the particle size (nm) and number (%) of $ZnAl_2O_4$ spinel particles at reaction temperature of 300°C

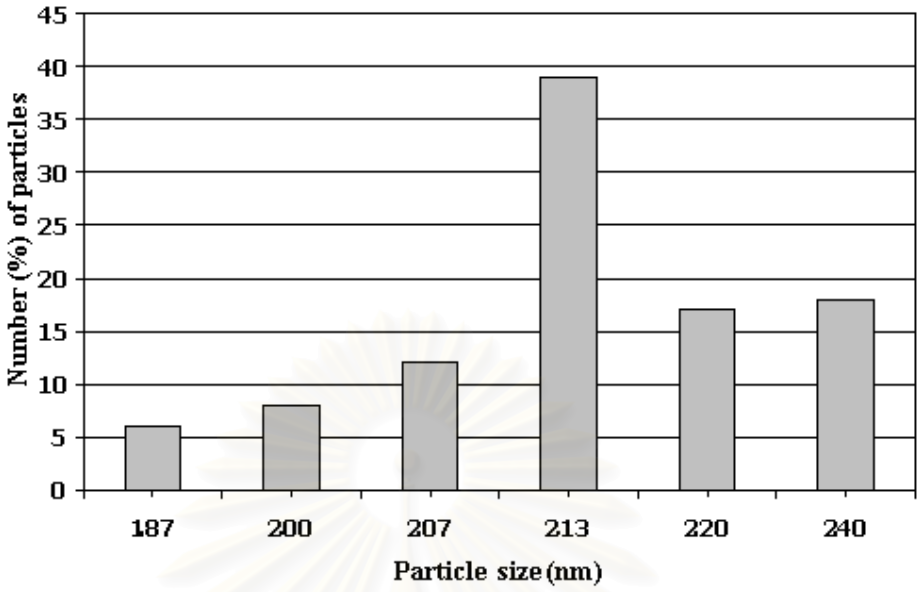

Figure E.3 The relation between the particle size (nm) and number (%) of $NiAl_2O_4$ spinel particles at reaction temperature of 300°C

VITA

Miss Angkana Kanyanucharat was born on July 11, 1978 in Bangkok, Thailand. She received the Bachelor Degree of Chemical Engineering from Faculty of science, Chulalongkorn University in 2000. She continued her Master's Study of Faculty of Engineering, Chulalongkorn University in June 2000.